Proceedings of:

Mechanical Metrology and Measurement Uncertainty

2009 Spring Topical Meeting

April 6 and 7, 2009

DoubleTree Hotel Albuquerque
Albuquerque, New Mexico

The American Society for Precision Engineering (ASPE) is a multidisciplinary professional and technical society concerned with research and development, design, manufacture and measurement of high accuracy components and systems. ASPE activities encompass relevant aspects of mechanical, electronic, optical and production engineering, physics, chemistry, and computer and materials science. Membership is open to anyone interested in any aspect of precision engineering.

Founded in 1986, ASPE provides a new focus for a diverse but important community. Other professional organizations have covered aspects of precision engineering, always as a sideline to their principal goals. ASPE is based on the core of generic concepts necessary to achieve precision in any application; independent of discipline, ASPE intends to be the focus for precision technology, and to represent all facets from research to application.

ASPE – The American Society for Precision Engineering
301 Glenwood Avenue, Suite 205, Raleigh, NC 27603
P.O. Box 10826, Raleigh, NC 27605
Telephone: (919) 839-8444 Fax (919) 839-8039
Web site: http://www.aspe.net

Preface

This book comprises the proceedings of the 2009 Spring Topical Meeting. The contributions reflect the authors' opinions and are published as presented to ASPE, without change. Their inclusion in this publication does not necessarily constitute endorsement by the ASPE, or its editorial staff.

Individual readers of this book and nonprofit libraries acting for them are permitted to make fair use of the material contained in this book to be used in teaching or research; provided they copy said paper in total, as written by the author. Permission is granted to quote excerpts from the scientific or technical works in this book with proper acknowledgment of the source to include: The author's name, the book name, and the ASPE tag line. Reproduction of figures and tables is likewise permitted from the contents of this book, provided that the same acknowledgment of the same source and content is permitted.

Any other type reproduction, systematic copying or multiple reproduction of any material in this book is expressly prohibited except with the written permission of the ASPE editorial staff, addressed to the Society's headquarters.

ISBN 978-1-887706-49-0

2009

American Society for Precision Engineering
301 Glenwood Avenue, Suite 205
Raleigh, NC 27603

Printed in the United States of America

2009 Spring Topical Meeting

Contents

Preface ..... *ii*

Contents ..... *iii*

Program ..... *iv*

Foreword ..... *v*

Technical Paper Index ..... *vi*

Technical Papers *3-55*

Author Index *57*

2009 Spring Topical Meeting

Meeting Schedule

	Monday, April 6	Tuesday, April 7
7:30	**Registration**	
8:45	**WELCOME REMARKS**	
9:00 10:15	TECHNICAL SESSION I	TECHNICAL SESSION V
	Coffee Break	
10:45 12:00	TECHNICAL SESSION II	TECHNICAL SESSION VI
	Lunch	
1:30 2:45	TECHNICAL SESSION III	OPEN DISCUSSION AND WRAP-UP
	Refreshment Break	
3:15 4:30	TECHNICAL SESSION IV	
	Free Time	
5:00 6:00	CASUAL RECEPTION	
6:00	FREE EVENING (Dinner on your Own)	

Foreword

Physical and mechanical metrology encompasses many applications. Examples of physical metrology include pressure and vacuum metrology; flow metrology, from the leaks regime (10^{-12} cm^3/s) to larger flow rates (10^4 cm^3/s); measurement of thermodynamic quantities such as temperature and humidity; mass metrology, and dimensional metrology. In many cases, capabilities in one area are critical to the traceability of measurements in a different area: For example, many pressure measurements ultimately rely on the determination of the mass of a deadweight, and on the measurement of the area of a piston. In another example, the traceability for the impedance of microwave air lines relies on dimensional measurement of the air lines.

This meeting (jointly held with the Albuquerque section of the NCSLI) focuses on precision engineering applications to metrology, metrology practices, and calibration practices.

2009 Spring Topical Meeting Program Committee:

Meeting Co-Chairmen:

Hy D. Tran
Sandia National Laboratories

John R. Stoup
National Institute of Standards and Technology

Technical Organizing Committee:

James G. Salsbury
Mitutoyo America Corporation

Edward P. Morse
University of North Carolina at Charlotte

Technical Sessions

Introduction and Welcome

Monday, April 6, 2009, 8:45 am - 9:00 am

1. ***Welcome and Introductory Remarks***
   Hy D. Tran (Sandia National Laboratories); John R. Stoup (National Institute of Standards and Technology)

Session I
Developments in Metrology Equipment and Techniques - Part I

Monday, April 6, 2009, 9:00 am - 10:15 am

1. ***Accurate Picometers for DC and Low-frequency Displacement Measurement***
   Pratt, J. R.; Smith, D. T. (National Institute of Standards and Technology); and Howard, L. P. (Precera, Inc.) 3
2. ***Full Area Calibration of Large Optical Flats***
   Evans, C. J.; Smith, C.; Soobitsky, J. A.; Woynar, M. (Zygo Corporation) 7

Session II
Developments in Metrology Equipment and Techniques - Part II

Monday, April 6, 2009, 10:45 am - 12:00 pm

1. ***Tactile and Optical Cylinder Calibration with Nanometer Uncertainties***
   Jusko, O. E.; Bastam, D.; Reimann, H. (Physikalisch-Technische Bundesanstalt) 11
2. ***Isara 400: Development of an Ultra-precision CMM for 3D Measurement of Large Parts***
   Spaan, H. A. M.; Donker, R. L.; Widdershoven, I. (IBS Precision Engineering) 15

Session III
Case Studies in Mechanical Metrology – Part I

Monday, April 6, 2009, 1:30 pm - 2:45 pm

1. ***Swing Arm Optical CMM***
   Su, P.; Oh, C. J.; Parks, R. E.; Burge, J. H. (University of Arizona) 20
2. ***A Few Case Studies in Uncertainty Using the NIST M48 CMM***
   Stoup, J. R. (National Institute of Standards and Technology) 26

Session IV
Case Studies in Mechanical Metrology – Part II

Monday, April 6, 2009, 3:15 pm - 4:30 pm

2. ***Measurement of True Position of Threaded Holes***
   Bryce, E. A. (Sandia National Laboratories) 36
1. ***Uncertainty in Torque Calibration****
   Doiron, T. D. (National Institute of Standards and Technology) 40

* *Extended abstract unavailable at press time*

Casual Reception

Monday, April 6, 2009, 5:00 pm – 6:00 pm

Session V

Industry and Uncertainties – Part I

Tuesday, April 7, 2009, 9:00 am – 10:15 am

1. ***NCSLI Board of Directors Meeting Highlights ****
   Roger N. Burton (Honeywell FM&T) 41
2. ***Test Uncertainty in ISO TC213***
   Morse, E. P.; Khanam, S. A. (University of North Carolina at Charlotte) 42

Session VI

Industry and Uncertainties – Part II

Tuesday, April 7, 2009, 10:45 am - 12:00 pm

1. ***Test Uncertainty Ratio (TUR)***
   Khanam, S. A.; Morse, E. P. (University of North Carolina at Charlotte) 45
2. ***New Concepts in Uncertainty when Calibrating Measuring Equipment***
   Salsbury, J. G. (Mitutoyo America Corporation) 50

Session VII

Open Discussion and Wrap-up

Tuesday, April 7, 2009, 1:30 pm – 2:30 pm

* *Extended abstract unavailable at press time*

Technical Papers

Accurate Picometers for DC and Low-Frequency Displacement Measurement

J.R. Pratt[1] , D.T. Smith[1], and L.P. Howard[2]
[1]National Institute of Standards and Technology, Gaithersburg, MD 20899, USA
[2]Precera, Inc., Damascus, MD, 20872, USA

ABSTRACT

We have developed a fiber-optic interferometer optimized for best performance in the frequency range from DC to 1 kHz, with displacement linearity of 1 % over a range of ± 25 nm, and noise-limited resolution of 2 pm [1]. The interferometer uses a tunable infrared laser source (nominal 1550 nm wavelength) with high amplitude and wavelength stability, low spontaneous self-emission noise, high sideband suppression and a coherence control feature that broadens the laser linewidth and dramatically lowers the low-frequency noise in the system. The amplitude stability of the source, combined with the use of specially manufactured "bend-insensitive" fiber and all-spliced fiber construction, result in a robust homodyne interferometer system that achieves resolution of 40 fm·Hz$^{-1/2}$ above 20 Hz and approaches the shot-noise-limit of 20 fm·Hz$^{-1/2}$ at 1 kHz for an optical power of 10 μW, without the need for differential detection. Here we briefly review the design and construction of the interferometer, demonstrate its use for feedback stabilization of a probe displacement, and suggest a method to link the interferometer output to an absolute wavelength reference with an uncertainty on the order of 0.5% for displacements on the order of 100 pm.

FIBER INTERFEROMETER

The interferometer is shown schematically in Figure 1. The configuration is that of a simple fiber-optics-based, homodyne, single-detector interferometer; the components are in general the same as those described in Rugar et al. [2], with a few noteworthy modifications that are described in detail in Ref. [1]. Here, we highlight two important considerations that are required to achieve single-digit picometer resolution.

As described in Ref. [2], fairly broad spectrum, multi-mode diode laser sources are used for fiber interferometers because systems based on long-coherence-length light (e.g., narrow linewidth sources such as He-Ne lasers) were prone to spurious interference from stray reflections at optical interfaces. Such spurious interference is a known source of low-frequency noise. However, the remedy of using broad linewidth sources represents a compromise, since multi-mode diode lasers are prone to wavelength fluctuations that mimic a low-frequency displacement. In the work of Rugar *et al.* [2], this compromise manifested itself as linearly increasing noise as a function of fiber-to-reflector spacing, which led to the notion that for noise performance better than 10 pm, the fiber-to-reflector spacing must be kept below 5 μm, greatly limiting the applicability of the technique.

The system of Figure 1 solves this problem by employing a light source that exhibits both stable mean frequency and broad linewidth (e.g., "coherence control"). Using this latest generation light source the low-frequency performance of the interferomter is effectively decoupled from fiber-to-reflector spacing. Of course, several other critical design steps are employed to minimize low-frequency noise, which are beyond the scope of this paper (see Ref. [1] for a complete description). But as an example, consider that single-mode fibers tend to scatter light into the fiber cladding as they flex, resulting in bending-loss. Such intensity changes in a homodyne system are interpreted as displacements, and to minimize intensity fluctuations from fiber flexing we therefore resorted to a specially manufactured bend-insensitive fiber. We found that using this bend-insensitive, jacketless fiber significantly reduced the noise content in the 1 Hz to 20 Hz region when the interferometer signal was viewed on a spectrum analyzer; a simple 25 mm diameter mandrel-wrap test using an optical power meter showed a factor of 26 improvement over non-bend-insensitive fibers such as SMF-28.

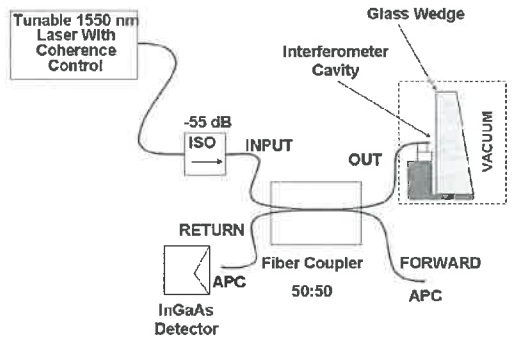

FIGURE 1. Schematic diagram of the fiber-optic interferometer showing the laser, optical isolator (ISO), evanescent wave coupler, single InGaAs detector and the interferometer cavity (note, APC means angle polished connector).

FEEDBACK STABILIZED PROBE

The feedback-stabilized probe instrument we consider here provides unprecedented stability and accurate dimensional measurement for the study of atomic point contacts by combining the positioning capabilities of a scanning tunneling microscope (STM) with the exceptional stability of a mechanically controlled break junction system [3]. The instrument is essentially an STM equipped with the fiber interferometer, which forms a cavity immediately adjacent to the probe (see Figure 2).

The probe and optical fiber assembly are positioned relative to a Au flat using two piezoelectric nanopositioners capable of both linear step motion over 5 mm and fine extension with sub-picometer control in vacuum at 4 K. One positioner moves the plate supporting the probe and fiber normal to the Au flat (the "*z*-axis" direction). The second positioner moves the Au flat perpendicular to the *z*-axis (the "*x*-axis" in Figure 2), allowing us to move to new positions on the Au flat as needed. The entire assembly is mounted to a base plate at the center of an inexpensive commercial cryogenic vacuum probe station chamber.

By using the interferometer output to control the *z*-axis positioner, the instrument can actively maintain a constant separation between the Au surface and the fiber end (and therefore the probe tip). The bandwidth of the servo-control loop (a commercially available analog proportional, integral, and derivative controller) is limited by the positioner dynamics to approximately 200 Hz, but this is sufficient for the cancellation of drift and low-frequency seismic and air-handling vibrations. For cavity lengths in the range 5 μm to 40 μm, we have determined that the interferometer resolution is noise-limited at 2 pm for quasistatic cavity measurements and at approximately 40 fm when low frequency (< 20 Hz) modulation is employed [1]. When changing the position set point in the control loop, cavity length changes as small as 5 pm can be clearly resolved; Figure 3 shows measured changes in cavity length resulting from set point changes.

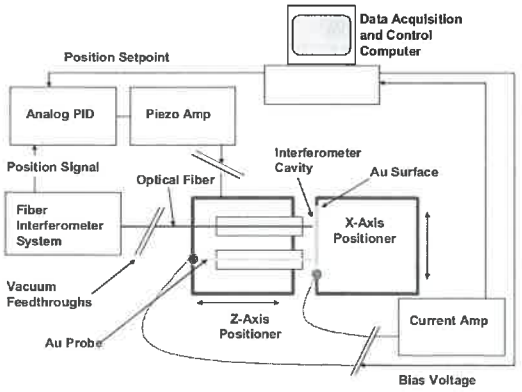

FIGURE 2. Probe system layout.

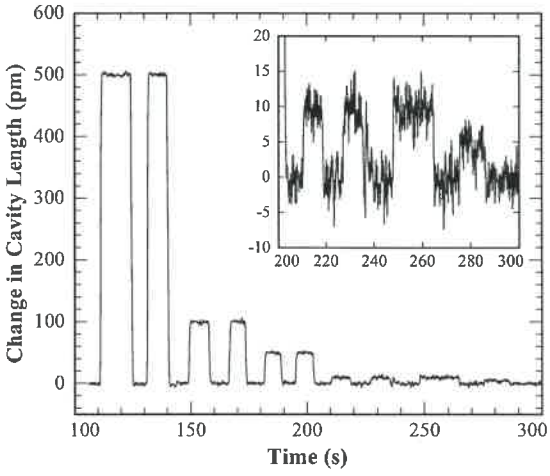

FIGURE 3. Observed changes in the interferometer cavity length as the servo control set point is changed. Set point changes as small as 5 pm produced well-defined changes in the cavity length. The data were taken in vacuum at 4 K.

DISPLACEMENT CALIBRATION

For a classical two-beam (TB) interferometer, interference produces sinusoidal "fringes" in both the transmitted and reflected light as the cavity length is varied. The normalized reflected intensity (for perfect visibility, discussed below) is given by [4]:

$$\frac{I_r(TB)}{I_p(TB)} = \frac{1}{2}\left[1 - \cos\left(\frac{2\pi\Delta L}{\lambda}\right)\right] \qquad (1)$$

where the reflected intensity, I_r, at wavelength λ is normalized by the peak reflected intensity, I_p, and ΔL is the path length difference between the two beams. (Paths are assumed to be in vacuum, and have an index of refraction n = 1.000.) The sensitivity, S, of the system is then the change in detected intensity for a given change in ΔL, and is proportional to the derivative of Eq. 1. Maximum sensitivity occurs at the inflection, or quadrature, points on the fringes, where $I_r/I_p = 0.5$, and the phase angle $\varphi \equiv 2\pi\Delta L/\lambda = (2m+1)\pi/2$, for m an integer. Because in this work intensities are realized experimentally as voltages from photodetector amplifier circuits, we will switch notation such that V_{max} corresponds to Ip, where V_{max} is the detector output voltage at Ip, V_r corresponds to detector voltage for reflected intensity I_r, and $V_q = V_{max}/2$ is the detector voltage at quadrature. The sensitivity at quadrature, in terms of a detector voltage change for a given length change in ΔL is then given by:

$$S(TB) = \frac{\partial V_r}{\partial \Delta L} = \frac{2\pi V_q}{\lambda_q}, \qquad (2)$$

where λ_q is the wavelength at quadrature. $S(TB)$ has units of V/m. This linearized sensitivity is valid only for small perturbations of the cavity from quadrature, and it should be clear that in this mode of operation the interferometer is intended for measuring displacements of a few tens of nanometers or less.

For a Fabry-Perot (FP) cavity formed between a pair of parallel air-glass or vacuum-glass interfaces the situation is more complicated. Here the equivalent to path length difference, ΔL, is now $2h$, where h is the cavity length. Normalized reflected power is given by the reflection coefficient $R = I_r/I_p$, and is approximately 0.04 for a single air/glass interface. Again, we take the case where the cavity is vacuum, with an index of refraction 1.000, and the cavity endfaces are glass. The reflected intensity from the cavity as a whole having interfaces with reflection coefficient R is no longer a sinusoidal function of h. Instead, it is given by the Airy function [5]:

$$\frac{V_r(FP)}{V_p(FP)} = \frac{(1+R)^2}{2}\left[\frac{1-\cos\left(\frac{4\pi}{\lambda}h\right)}{1+R^2-2R\cos\left(\frac{4\pi}{\lambda}h\right)}\right]. \qquad (3)$$

One consequence of this correction to the TB case is that the phase angle $\varphi = 4\pi h/\lambda$ at which $V_r/V_p = 0.5$ is no longer given by $(2n+1)\pi/2$ for integer n, but has shifted slightly. For $R = 0.04$, the phase angles where $V_r/V_p = 0.5$ become $\varphi = [(2n+1)\pi/2][1+(-1)^n 0.083]$.

As in the two-beam case above, the sensitivity of the interferometer to changes in h is determined from the derivative of normalized intensity. Taking the derivative of Eq. 3 with respect to h we find:

$$\left(\frac{\partial}{\partial h}\right)\frac{V_r(FP)}{V_p(FP)} = \frac{2\pi(1+R)^2}{\lambda}\left[\frac{(1-R)^2\sin\left(\frac{4\pi}{\lambda}h\right)}{\left[1+R^2-2R\cos\left(\frac{4\pi}{\lambda}h\right)\right]^2}\right]. \qquad (4)$$

Evaluating this expression with $R = 0.04$ for those phase angles φ where $V_r/V_p = 0.5$ [note when comparing $S(FP)$ to $S(TB)$ that ΔL corresponds to $2h$], we see that the sensitivity $S(FP)$ of our FP interferometer at $V_q = V_{max}/2$ is:

$$S(FP) = 1.003 \cdot S(TB) = 1.003 \cdot \left(\frac{4\pi V_q}{\lambda_q}\right). \qquad (5)$$

It also is noted that the condition $V_q = V_{max}/2$ does not correspond exactly to the maximum possible sensitivity for a FP cavity, as determined from the maximum of Eq. 4, but for R small it is close to optimal, and serves as an

experimentally convenient and reproducible set-point. It is further noted than for the derivation of S(FP) above, it is assumed that the reflection coefficient R from both glass/air interfaces is the same, so that the detected output voltage V_{min} at a fringe minimum is very close to zero, as was the case in experiments.

The light source for our interferometer can be tuned stably and accurately over the wavelength range 1440 nm to 1640 nm. This tuning range enables two very convenient operational features. First, when we either have no control over the macroscopic cavity spacing, as for example in the case of measuring the deflection of a cantilever force sensor, or we choose not to change the cavity out of concerns for dimensional stability, we can still operate the interferometer at its maximum sensitivity by tuning λ, so long as the cavity is large enough to contain a V_q within the tuning range of the laser. Second, we can make an absolute determination of a fixed cavity length h by sweeping wavelength. Since maxima in reflected intensity occur when $4h/\lambda = 2m+1$ for both TB and FP fringes, assuming no phase shift at the interfaces (other than standard phase inversion), and minima occur when $4h/\lambda = 2m$, it follows directly that h can be calculated from the measured wavelength values λ_m and λ_{m+1} of two consecutive fringe maxima or minima:

$$h = \frac{1}{2}\frac{\lambda_m \lambda_{m+1}}{(\lambda_{m+1} - \lambda_m)}. \qquad (6)$$

For the tuning range of our laser, this means that we can make an absolute determination of cavities as small as h = 6 µm. If a consecutive maximum and minimum are used to calculate h, 3 µm cavities can be measured. Accuracy is limited by our ability to measure λ_m and λ_{m+1}. With curve fitting, wavelengths of maxima and minima can typically be determined within a range of ± 0.1 nm, permitting cavity length determination to better than one part in 1000.

Laser tunability also permits an independent check on the sensitivity given in Eq. 5 that can be linked to International System of Units (SI). The procedure is as follows. A cavity length and laser wavelength are selected such that the detector output is $V_q = V_{max}/2$ for wavelength λ. The cavity length h is then changed by a small amount ε, and the new output voltage ($V_q + \Delta V$) is recorded. The change ε in cavity size does not need to be known, provided that $\varepsilon \ll \lambda/2$. The laser wavelength is then tuned to a new wavelength ($\lambda + \Delta\lambda$) such that once again $V_q = V_{max}/2$. For a known cavity length h and fringe order m, it is then possible to relate ε to the actual cavity length change Δh and determine the sensitivity $\Delta V/\Delta h$. Subsequent displacement measurements made with such a system can thus be made traceable through SI-traceable laser wavelength calibration [6]. The procedure is straightforward, but assumes an unambiguous and monotonic relation between wavelength and measured intensity. At present, this procedure is limited in this set up to perhaps 0.5% relative uncertainty due to systematic fluctuations in the interferometer intensity (see Ref [1]).

CONCLUSIONS

We have developed an exceptionally stable experimental platform for the study of atomic scale contacts by placing an interferometer cavity directly adjacent to a probe. This allows us to close a servo loop around the junction separation with picometer stability, so as to remove thermal drift and low-frequency vibration artifacts. The system could greatly improve a number of contact, or near-contact, atomic-scale experiments, allowing direct and accurate measurement of the probe displacement with respect to the surface. In addition, future work will incorporate a second interferometer and a stiff elastic force sensor, such that direct measurements can be made of bond stiffness and breaking force. The interferometer design currently being used for measuring probe motion provides sufficient sensitivity for measuring the deflection of a stiff (> 100 N m^{-1}) cantilever force sensor.

REFERENCES

[1] Smith, D.T., Pratt, J.R., Howard, L.P., Rev. Sci. Instrum., **80**, 035105 (2009).

[2] D. Rugar, H.J. Mamin, and P. Guethner, Appl. Phys. Lett. **55**, 2588 (1989).

[3] Smith, D.T. and Pratt, J.R., Applied Physics Letters, submitted, (2009).

[4] M. Born and E. Wolf, *Principles of Optics*, Third Revised Edition, Pergamon Press (1964).

[5] J.L. Santos, A.P. Leite, and D.A. Jackson, Applied Optics 31, 7361 (1992).

[6] S.L. Gilbert, W.C. Swann and C.-M. Wang, NIST Special Publication 260-137, 2005 Edition.

FULL AREA CALIBRATION OF LARGE OPTICAL FLATS

Chris Evans, Craig Smith, Jim Soobitsky and Michael Woynar

Zygo Corporation
Middlefield CT 06455, USA

INTRODUCTION

Full area calibration of the transmission flat (TF), or reference surface, of a 450 mm aperture plano interferometer has been performed with an estimated expanded uncertainty (k=2) of less than 3 nm. Cross-check measurements are consistent with the uncertainty analysis. First we will briefly review the calibration method. Then we will present selected data, and finally discuss the uncertainty analysis.

METHOD

Pairwise intercomparison of three flats has long been the method of choice for providing "flatness" calibrations. Such calibrations are valid only along profiles. Over the last 25 years, a number of variants on the 3-flat test which provide area calibrations have been described in the literature and used on small to medium sized flats. All these methods require moving flats with respect to one another and most require rotation of at least one of the flats. Evans and Kestner[1] briefly reviewed available methods and then described a 2-dimensional analog of the classic multi-position roundness test to evaluate the rotationally varying (RV) components of the flats under test and showed how that could be used to provide an area solution. Briefly, if one of the flats is rotated to N positions separated by 360/N degrees, then the average of these N measurements contains none of the RV terms associated with the rotating flat, except those at azimuthal frequencies of kNθ, where k is a positive integer. With appropriate hardware and time, rotations may be used in more than one cavity, adding redundancy to the solutions.

As the flats get larger, practical difficulties associated with the calibrations increase rapidly; in particular, all the methods assume that the flats do not change figure due to handling and mounting in different locations and orientations during the test. A procedure using the minimum set of measurements, when the rotatable flat is a TF, appears elsewhere[2]. For the case where there are two TFs (A and B) and a rotatable return flat (RF) denoted here as C, we can express the individual measurements in terms of the rotationally invariant (RI) and RV components, for example:

$$AB = A_{RI} + A_{RV} + B_{RI} + B_{RV}^{180}$$

where the first letter represents the TF on the interferometer. The data are assumed to be in detector coordinates, hence the contribution of B is flipped, as indicated by the superscript, noting that flipping the RI term causes no change in the result. Taking inspiration from the "classic" 3-flat test, it is easy to show that:

$$\frac{AB + AC - BC}{2} = A + \frac{(B_{RV}^{180} - B_{RV})}{2}$$

The difference between the measurement BC and the average of all measurements with C at the N different azimuthal positions is:

$$\begin{aligned} BC - BC_{ave}^{R} &= (B_{RI} + B_{RV} + C_{RI} + C_{RV}^{180}) \\ &\quad -(B_{RI} + B_{kN\theta} + C_{RI} + C_{RV}^{180}) \\ &= B_{RV} - B_{kN\theta} \end{aligned}$$

which can be substituted for BRV and its flipped version, BRV^{180} , giving a solution for A. The value of N is chosen to make the bias arising from the kNθ term acceptably small [3]. Results for the surfaces of B and C are obtained by subtracting the calibrated value of A from the AB and AC cavities.

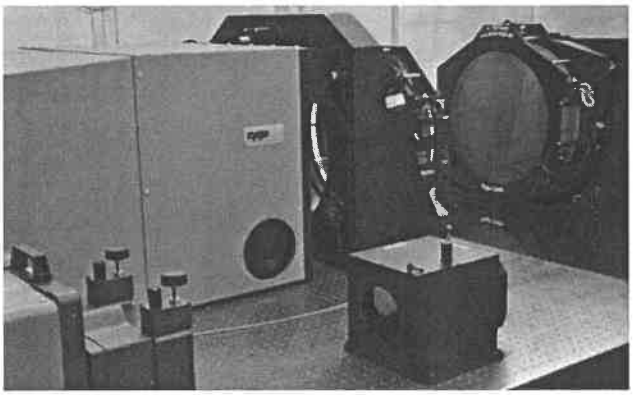

Figure 1: Measurement set-up

IMPLEMENTATION

Figure 1 shows the calibration set-up in a temperature controlled (+/- 0.01C) metrology laboratory, with the mainframe interferometer (lower left), beam expander and test cavity. Custom high stability mounts ensure that the TFs can be removed and replaced with a low order figure change of less than 1.5 nm peak to valley. The oversized calibration RF is mounted so that it can easily be rotated without the operator touching the glass, minimizing thermal transients during the calibration.

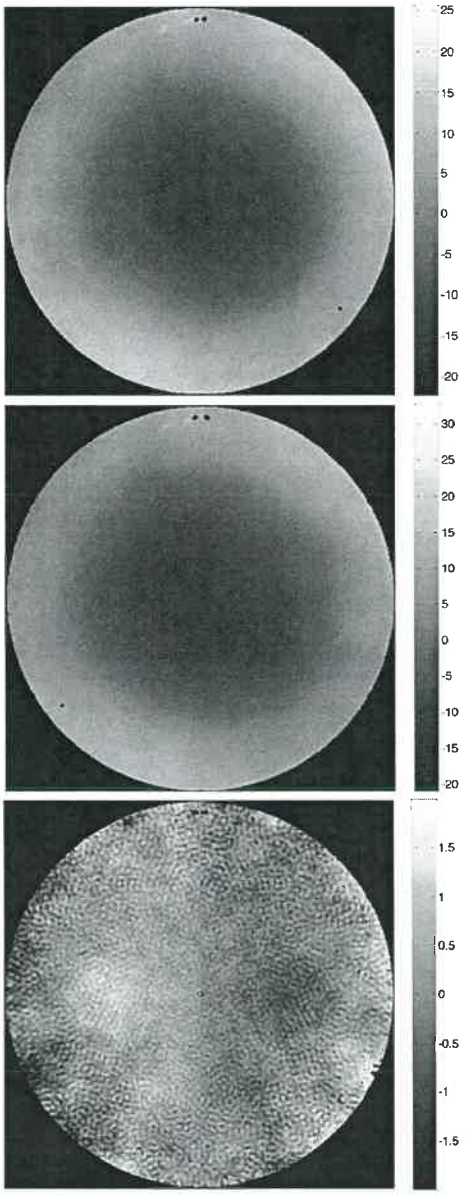

Figure 2: Two independent calibrations of A: (top): PVr = 32.6 nm, rms = 8.6 nm; (center) PVr = 32.3 nm, rms = 8.6 nm; (bottom) difference, rms = 0.6 nm

RESULTS

Figure 2 shows two independent calibrations of one of the TFs. The two calibrations were made with different numbers of rotational positions (N=5 and 6 respectively) and with the rotation performed with respect to different TFs (ie AC(N=5) and BC(N=6)). Different algorithms to reduce the two data sets were required, leading to different data drop out from the fiducials in the two measurements. The agreement between amplitude parameters for the calibrations (rms and PVr[4]) is 0.3 nm.

The raw data contains outliers, resulting for example from diffraction at the edge of fiducials or from minor defects in the interferometer. These have been removed from the difference plot, to allow the residual structure to be seen. Note the left right symmetry of this plot, which indicates a small error in the location of the flip axis when flat B is moved between TF and RF positions. The difference between the 2 maps has an rms of 0.6 nm.

A simple check measurement derives from the nature of the algorithm. Since B and C are computed by subtracting the calculated value of A from the AB and AC cavities, any error in A (including the $kN\theta$ term) leads to an equal and opposite error of the same sign in both B and C. Hence, subtracting the calculated maps for B and C from the measured BC cavity gives twice the error (for most errors) plus some noise; the exception is an error in the BC cavity before any rotations which is heavily attenuated in the check measurement. In all the calibrations performed, the rms of the check measurement was less than 1 nm.

As noted in the previous paragraph, the procedure results in calibration of 2 TFs. Hence, another check is to measure a fourth flat with both the calibrated TFs. Figure 3 shows the results of such measurements of a flat not used in the calibration process. The rms of the difference map is 0.5 nm.

UNCERTAINTY ANALYSIS

Traditionally, flatness is expressed as the peak to valley (PV) departure after removal of a best fit plane. Elsewhere we have shown that PV is a biased estimator [5]. Furthermore, a common purpose of the type of calibration described here is to generate a reference file to subtract from subsequent measurements (eg Figure 3). Hence, the measurand might more properly be

considered to be the surface map, and the uncertainty a matrix of the same size. Haitjema showed some low density matrices in the measurement of surface plates[6]. The first published use of an uncertainty matrix in optical testing appears to be for wafer thickness metrology[7].

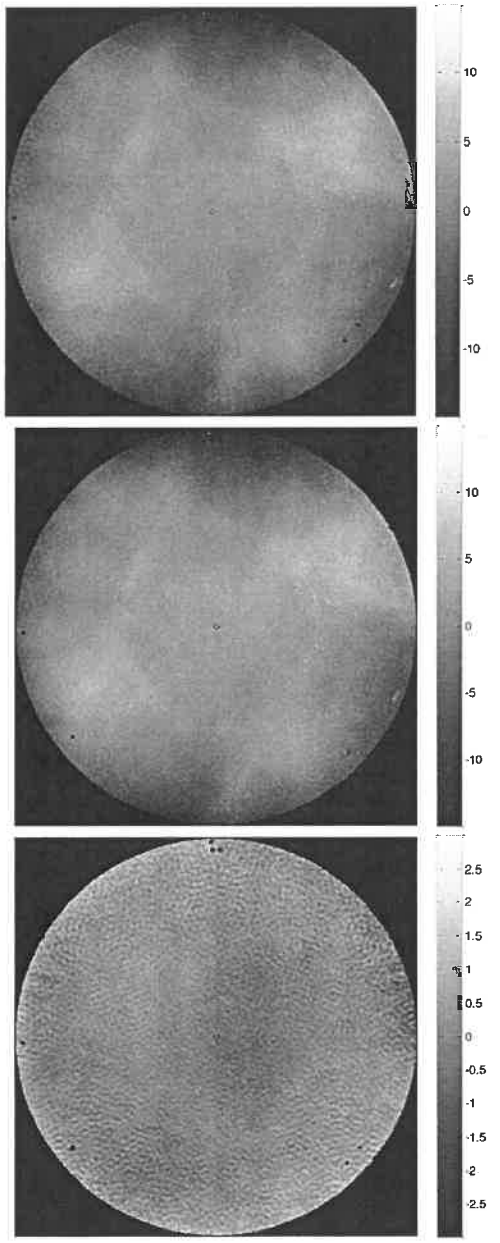

Figure 3: Measurements using the two calibrated TFs: (top) PVr = 23.8 nm, rms = 3.7 nm; (center) PVr = 24.3 nm, rms = 3.9 nm; (bottom) difference, rms = 0.5 nm

Our approach to generating the uncertainty matrix follows the ISO Guide to the Expression of Uncertainty in Measurement [8].Type A uncertainties are evaluated experimentally; for each of the individual measurement set-ups (ie AB, AC and all the rotated positions of BC) 20 individual phase maps are acquired and the standard deviation per pixel computed and combined according to the measurement model (Figure 4). Note that a small number of pixels, for example those associated with an on-axis "hot-spot", drive the range.

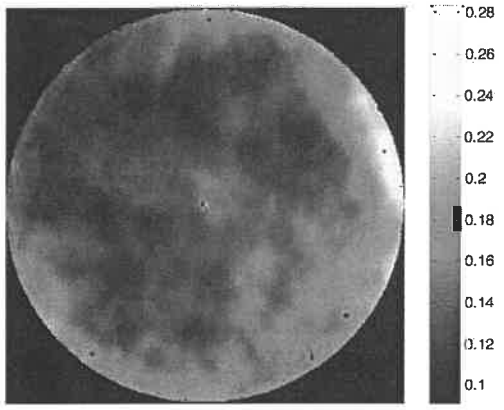

Figure 4 Combined Type A uncertainties, outliers removed from plot but not from statistics; mean = 0.14 nm, max = 3.8 nm.

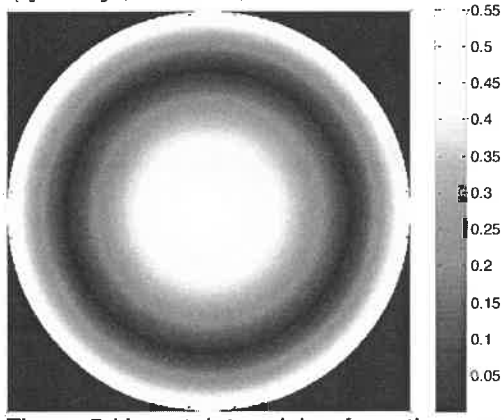

Figure 5 Uncertainty arising from the uncertainty in the axial temperature gradient in the TF

Uncertainties that we choose not to treat statistically (Type B) are those that are time invariant or where the variation is slow compared to the data acquisition time. Some are treated analytically from first principles[5]. Others are treated by establishing sensitivities using the calibration result itself. For example, Figure 5 shows the uncertainty arising from an axial temperature gradient calculated from

simple bending theory and an assessment of the range of probable values for the temperature gradient. Figure 6 shows the uncertainty resulting from uncertainty in the orientation in rotation of B when used in the two different positions – as TF or RF. This matrix results from evaluating the range of probable value of the rotation and the result of small angle rotation of the calibration result for the flat in question

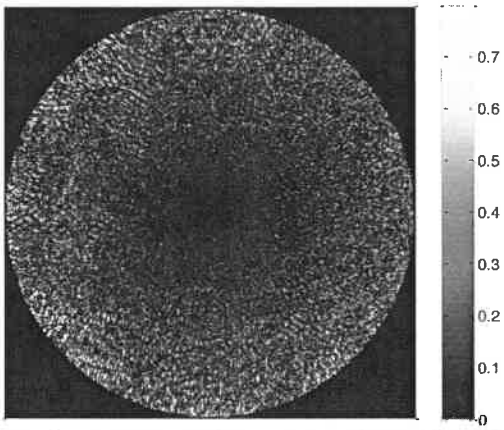

Figure 6 Uncertainty arising from uncertainty in the rotational orientation

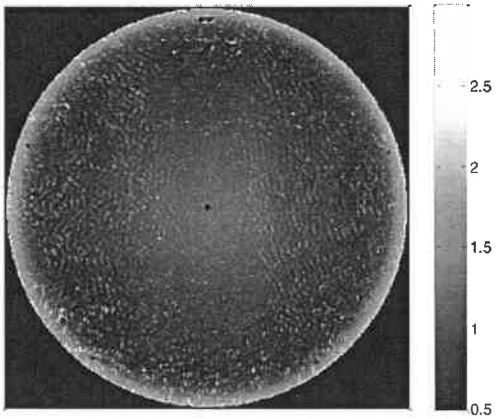

Figure 7 Expanded uncertainty matrix (k=2) for in-situ calibration of a TF

Clearly, many of these uncertainty matrices show spatial correlations. Fortunately the influence quantities are uncorrelated. Hence the combined standard uncertainty matrix is computed by summing in quadrature (rss) pixel by pixel. Figure 7 shows the expanded uncertainty matrix (k=2).

There are a number of possible approaches to single number quantification of uncertainty matrices. The peak value is clearly driven by outliers in the Type A uncertainty matrix. Use of the mean might seem convenient, but understates the range of probable values of the surface form in some parts of the aperture. A conservative parameter is the 99.5th percentile, which indicates the range without being driven by outliers. The 99.5th percentile of the data in Figure 7 is 2.2 nm.

CONCLUSION

We have demonstrated full area calibration of flats with apertures up to 450 mm with nm level uncertainty. Such in-situ calibration, and reference error subtraction, is essential to achieve the highest quality optics manufacturing. Minimizing test uncertainty also maximizes the manufacturing headroom for any given target specification.

References

[1] Evans C. J. and Kestner R.N. Test Optics Error Removal. Applied Optics, **35** (1996) , pp1015-21

[2] Evans C. J. Comment on the paper "Interferometric testing of optical surfaces: absolute measurement of flatness". Optical Engineering, **37**(1998) pp1880-82.

[3] Parks R.E., Evans C.J., Sullivan P. J., Shao L-Z, and Loucks B. Measurement of the LIGO Pathfinder Optics. Proc SPIE, Optical Manufacturing and Testing II, (ed H. P. Stahl), Vol 3134 (1997), pp95-112.

[4] Evans C. J. PVr – a robust amplitude parameter for optical surface specification. Optical Engineering, in press, 2009

[5] Evans C. J. Uncertainty evaluation for measurements of peak to valley surface form errors. CIRP Annals, Vol 57/1 (2008), pp509-12

[6] Haitjema H., 1992, Uncertainty Propagation in Surface Plate Measurement, Proc. 4th Int. Symp. On Dimensional Metrology in Prod. And Qual. Control, 304-320

[7] Schmitz T.L., Davies A., Evans C. J., Parks R. E. 2003, Silicon Wafer Thickness Variation Measurements using the National Institute of Standards and Technology Infrared Interferometer, Optical Engineering, 42, 2281-2290.

[8] ISO Guide to the Expression of Uncertainty in Measurement, 1995

TACTILE AND OPTICAL CYLINDER CALIBRATION WITH NANOMETER UNCERTAINTIES

Otto Jusko, Dirk Bastam, Helge Reimann
Department Coordinate Metrology
Working Group Geometrical Standards
Physikalisch-Technische Bundesanstalt (PTB), Braunschweig and Berlin
38116 Braunschweig, Germany

INTRODUCTION

The calibration of cylindrical work-pieces and standards can be attached major importance, because most industrial work-pieces are cylindrical. Therefore various measurement instruments and measurement procedures have been developed to improve measurement uncertainty, measurement throughput, and data density for inner and outer cylinders [1].

This paper will describe a calibration procedure and measurement uncertainty analysis for cylinders by mainly focusing on piston-cylinder assemblies. However, the techniques are also applicable for cylinders of the same quality class.

DIMENSIONAL CALIBRATION OF PISTON-CYLINDER ASSEMBLIES

An important category of cylindrical work-pieces are piston-cylinder assemblies (also piston-cylinder units = "PCU") as utilized in pressure balances. These balances deal as primary gas standards. The diameter of such PCUs typically varies between 25 mm and 50 mm. In the last decade various procedures have been developed to calibrate these kind of standards dimensionally [2, 3]. This is due to the fact that Dadson's theory allows the calculation of the effective area of the PCUs on the base of dimensional input data [4].

The efforts in this field were increased since several NMIs including PTB started a joint project to re-determine Boltzmann's constant k_B. As k_B is the physical link between thermal and mechanical energy, the project may lead to a new definition of the Kelvin [5]. The chosen realization is based on a Dielectric Constant Gas Thermometer (DCGT) and such strongly depends on absolute pressure metrology. The target uncertainty for the pressure scale is $1 * 10^{-6}$. To achieve this goal the dimensional uncertainties have to be significantly lower than 50 nm. Recently, it was shown that these numbers can be achieved and even be superseded [6]. In the meantime new data and a more detailed uncertainty analysis became available. The utilized measurement equipment and procedures will be described below. Furthermore a detailed measurement uncertainty analysis is presented.

MEASUREMENT EQUIPMENT FOR TACTILE PROBING

For combined roundness, straightness and parallelism measurements a modified MarForm MFU8 (called MFU8PTB) was utilized [7]. This machine can also be used for size measurements, because PTB's version was extended by a plane-mirror interferometer.

High precision diameter measurements were performed with PTB's reference length comparator KOMF [8, 9]. It was shown that expanded measurement uncertainties in the range of less than 20 nm can be achieved with KOMF. This is mainly caused by the fact that the KOMF features two independent probes and interferometers and such allows a measurement strategy which is independent from a calibration of the contacting elements.

The MFU8PTB and the KOMF both are tactile i.e. mechanical contacting instruments. The same is valid for the new MFU110WP form measurement instrument, which also was utilized for these measurements. To eliminate influences from guidance errors and angle changes of the machine coordinate system during positioning the MFU110WP is equipped with a metrology frame, built up by two independent straight rules for the X- and Z-axis, respectively. These are monitored by four capacitance transducers each. Monitored guidance deviations incl. resulting angle (e.g. squareness) deviations are post-corrected by software.

OPTICAL PROBE SYSTEM

A unique feature of the MFU110WP is its optical i.e. non-contacting probe system, called WhitePoint. That system is based on a short coherence heterodyne interferometer working

with two wavelengths (1.55 µm, 36 µm) [10, 11]. WhitePoint optical probes may be used as full replacement for tactile probes. The shaft of the WhitePoint system, which carries also the optics, has a diameter of approx. 1.2 mm. In the MFU110WP the switching between the tactile and the optical probe may be performed manually by exchanging the probes physically or in case of combined optical / mechanical probes (Fig. 1) it may also be performed CNC-controlled by positioning of the swivel axis of the form measurement instrument.

FIGURE 1. Combined tactile and optical probe

There are several WhitePoint probes available. They offer different beam directions (e.g. 0°, 45°, 60°, and 90°) and / or numerical apertures. The swivel axis may also be utilized to select one of the beams (Fig. 2). As the optical probes are not limited by the stable mechanical probe-workpiece contact constraint as mechanical probes, they can be operated at much higher scanning speeds. In principle the scanning speed can be increased by approximately two decades. In practice, mechanical cross-talk from the axes drives, resonances of the probe shaft, and integration times of the optical system limit the usable scanning speed improvement to approximately one decade.

When the MFU110WP machine control is programmed for simultaneous movement of the rotary and the Z-axis, a helical trace on the workpiece can be scanned. This measurement mode is especially useful for the optical measurement system. This mode can be used for full 3D-cylinder surface scans (Fig. 3). A further important application is measuring a multiple revolution helical trace with short Z-travel distance of only some 10 µm to 100 µm. The resulting cylindrical data may be collapsed by the machine software to a single roundness trace. The main idea behind this function is to integrate spatially over the axial length to improve the match between tactile and optical scans. It may also be used to improve the signal-to-noise ratio. A comparison of tactile and optical data shows that the noise suppression is very effective and that the optical data are of the same or often superior quality than the tactile data (Fig. 4). Therefore this measurement mode was selected for all optical piston-cylinder measurements.

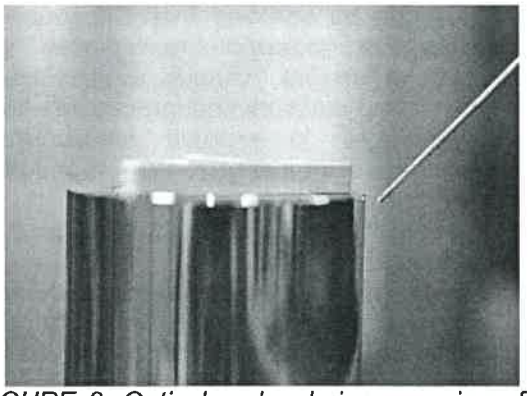

FIGURE 2. Optical probe during scanning of a cylindrical piston. The 45° beam exit was chosen.

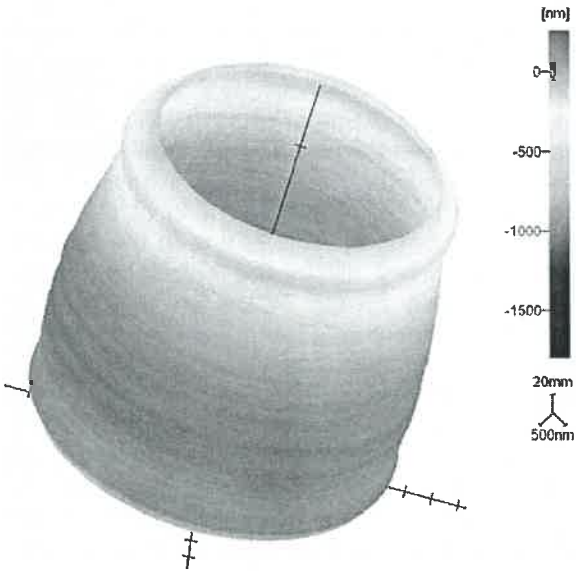

FIGURE 3. Helical 3D-scan of the full cylinder surface of the piston above

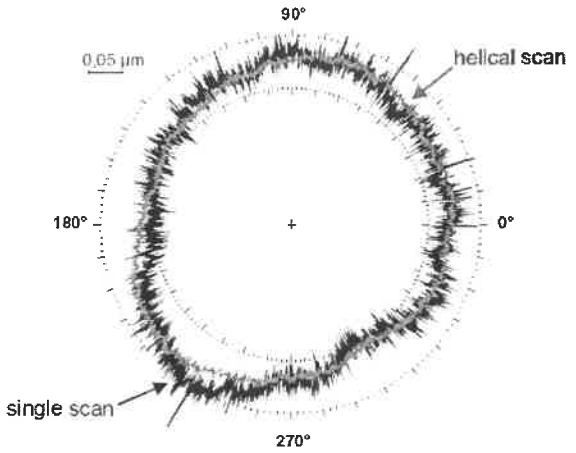

FIGURE 4. Collapsed helical roundness scan vs. single scan trace

DATA EVALUATION

The three-dimensional data set was generated from the straightness (S), roundness (R), and diameter measurements (D) by a least-squares best-fit procedure [12]. In contrast to earlier approaches, all diameter results were taken into account. For the actual evaluation equal weights were chosen for size and form data. The influence of individual weights for the fit procedure is still under evaluation. The fit-procedure outputs a table of fit discrepancies, which can be used as a benchmark for the consistency of the input data. Typical fit discrepancies are of the order 5 nm - 10 nm [13]. Fig. 5 shows the data cloud after the fit procedure has been applied.

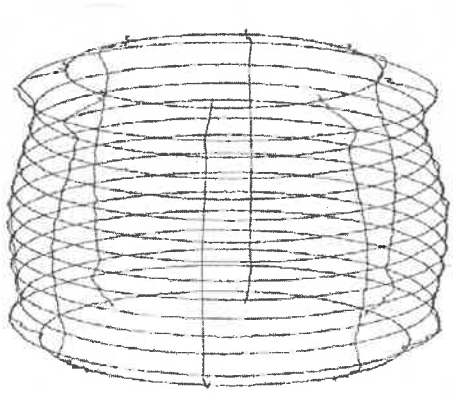

FIGURE 5. Visualization of a calculated 3D data cloud

UNCERTAINTY CALCULATION

The most important contributor for the resulting uncertainty of the 3D data is the diameter measurement uncertainty. The uncertainty budget for a KOMF diameter measurement can be found in Table 1. Details of the uncertainty calculation can be found in [9].

TABLE 1. Exemplary uncertainty budget for the diameter measurement of a piston by the length comparator KOMF . In this case the standard uncertainty amounts to u = 7.3 nm.

Input quantity Xi	**Sub-quantity**	**$u_i(y)$ / nm**
Exp. Std. dev.		**3.1**
LI Measurement		**2.8**
LI wavelength		**0.4**
Refractive index of air		**2.1**
Probing system measurement		**2.5**
Sensitivity of probing systems		**0.3**
Adjustment 1st order		**2.6**
	Abbe error	0.7
	Adjustment of probing spheres to each other	2.5
	Cresting	0.0
Adjustment 2nd order		**0.6**
	Adjustment of optics	0.5
	Adjustment of object	0.1
Material temperature		**2.6**
	Deviation from 20°C	2.6
	Drift of meas. frame	0.6
Influence of measurement object		**3.3**
	Roughness	2.9
	Form deviations	5.8
	Cleaning	0.0
	Elastic compression	1.7
Diameter of contacting sphere		**0.0**
Standard uncertainty of diameter		**7.3**

The uncertainties of the generatrix and circle trace radii in the resulting 3D data set were estimated based on the diameter uncertainties and taking into account the information of the applied least squares fit procedure for the 3D data set [12].

For outer cylinders (pistons) the resulting expanded uncertainty U (k=2) of the 3D data cloud amounts to 14 nm – 20 nm, in dependence of the individual PCU measurement objects.

For inner cylinders expanded uncertainties of 30 nm – 45 nm could be achieved.

CONCLUSIONS AND OUTLOOK

It was shown that combined tactile and optical 3D calibration of cylinders can be realized with nanometer uncertainties. Further work will concentrate on direct optical 3D calibration and full 3D cylinder surface calibration.

REFERENCES

[1] O. Jusko, M. Neugebauer, H. Reimann, High-Precision dimensional calibration of reference cylinders, Proc. Congress on Metrology, Measurement & Instrument Technology, IMEKO TC 14, 2001, I-7ff.

[2] O. Jusko., H. Bosse, F. Lüdicke, High precision 3D-calibration of cylindrical standards, in: Advanced Mathematical Tools in Metrology III (ed. by P. Ciarlini, M.G. Cox, F. Pavese and D. Richter), Singapore, World Scientific Publishing Company, 1997, pp. 186-194.

[3] M. Neugebauer, F. Lüdicke, D. Bastam, H. Bosse, H. Reimann and C. Topperwien, A new comparator for measurement of diameter and form of cylinders, spheres and cubes under clean-room conditions, Meas. Sci. Technol. 8 (1997) 849-856.

[4] R.S. Dadson, S.L. Lewis, G.N. Peggs, The Pressure Balance: Theory and Practice, London, HMSO, 1982.

[5] J. Fischer, B. Fellmuth, J. Seidel, W. Buck, Towards a new definition of the kelvin: ways to go, Proc. of the 9th Symp. on Temperature and Thermal Measurements in Industry and Science, TEMPMEKO, Dubrovnik Cavtat, Croatia, 2004, http:// www.imeko.org/publications/tc12-2004/PTC12-2004-PL-002.pdf.

[6] O. Jusko, M. Neugebauer, H. Reimann, W. Sabuga, T. Priruenrom, Dimensional Calibration Techniques for Pressure Gauges to be used in the new determination of the Boltzmann Constant, Proc. 1st International Congress on Mechanical Metrology, Rio de Janeiro, Brazil, 2008

[7] F. Lüdicke, O. Jusko, H. Reimann, Form and Length Measurements by Use of a Modified Commercial Form Measurement Instrument, ASPE Annual Meeting 2000, Scottsdale, AZ, USA

[8] M. Neugebauer, F. Lüdicke, A new comparator for measurement of diameter and form, in: Proc. of the 9th IPES/UME 4 Int. Conf., Braunschweig, Germany, 1997, pp. 178-181.

[9] M. Neugebauer, The uncertainty of diameter calibrations with the comparator for diameter and form, Meas. Sci. Technol. 9 (1998) 1053–1058

[10] P. Drabarek, Interferometric measuring device for determining the profile or the pitch of especially rough surfaces, WO 99/44009 (1999)

[11] P. Drabarek, T. Gnausch, M. Fleischer, Measuring Machines with Interferometrical Stylus for Form Measurement of Precise Mechanical Parts, to be published in ASPE Annual meeting Proceedings. 2008, (in Precision Engineering)

[12] W. Sabuga, T. Priruenrom, An approach to the evaluation of dimensional measurements on pressure-measuring piston-cylinder assemblies, Proc. of 3rd Conference on Pressure Meas., IMEKO TC16, Merida, Mexico, 2007, http://www.imeko.org/publications/ tc16-2007/IMEKO-TC16-2007-074u.pdf

[13] O. Jusko, D. Bastam, M Neugebauer, H. Reimann, W. Sabuga, T. Priruenrom, Final Results of the Geometrical Calibration of the Pressure Balances to be used for the new Determination of the Boltzmann Constant, to be published in Proc. of ISMTII 2009, St. Petersburg

ISARA 400: DEVELOPMENT OF AN ULTRA-PRECISION CMM FOR 3D MEASUREMENT OF LARGE PARTS

Henny A. M. Spaan, Rilpho L. Donker, and Ivo Widdershoven
IBS Precision Engineering
Eindhoven, The Netherlands

INTRODUCTION

IBS Precision Engineering

For more than 15 years, IBS Precision Engineering (IBS PE) has been involved in the development and realization of special machines, in particular for metrology applications, as well as machine tool calibration and inspection systems. The latest development, the Isara 400, will provide ultra-precision 3D coordinate metrology for large parts.

Isara, history

In collaboration with Philips Applied Technologies, IBS PE previously developed the Isara CMM, an ultra-precision 3D Coordinate Measuring Machine, with a measuring volume of 100 x 100 x 40 mm, with a 1D measuring uncertainty of 15 nm. This first Isara CMM, see figure 1, was based on the design by Ruijl [1]. Similarly, other ultra-precision measuring machines [2,3] have been developed, and are seeing an increasing number of applications. These machines typically feature measuring ranges of no more than 100 mm.

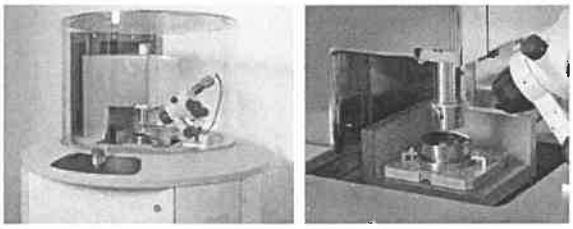

FIGURE 1. Photographs of the Isara CMM.

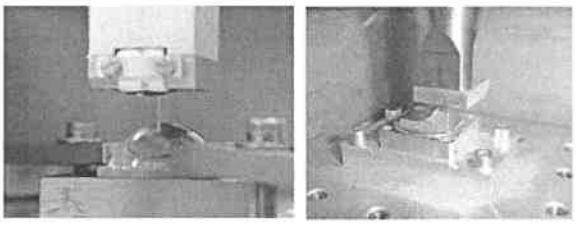

FIGURE 2. Examples of measured parts.

Examples of measured parts are shown in figure 2, results are shown in figure 3.

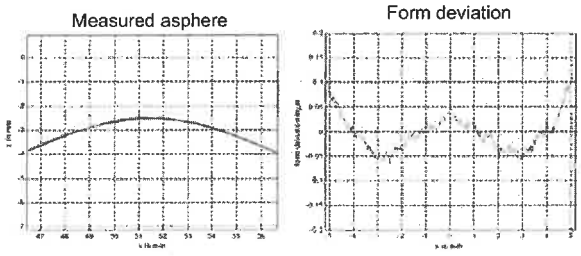

FIGURE 3. Results of asphere measurement.

The results of these measurements showed that the Isara CMM is capable of performing measurements on the nanometer level on complex optical parts. In response to the demand to enable 3D measurement of larger products with features that require nanometer measuring uncertainty, a new ultra-precision CMM, the Isara 400, is developed.

ISARA 400

Isara 400 Concept

The newly developed Isara 400 has a measurement volume of 400 x 400 x 100 mm, which is 40 times larger than the first Isara. The most important metrological design principle of the first Isara CMM, the Abbe principle [4], is maintained for the Isara 400. The Isara 400 conforms to this principle in 3D.
Three plane-mirror laser interferometers are applied as measuring systems for the machine axes. The interferometers each measure against one of the mirrors of a mirror table, on which the work piece is mounted. These interferometers are all mounted in a single metrology frame, which also holds the probe system, see figure 4.
The laser beams are aligned to the probe tip and their mutual alignment does not change, thus fulfilling the Abbe principle in 3D within the complete measuring volume.

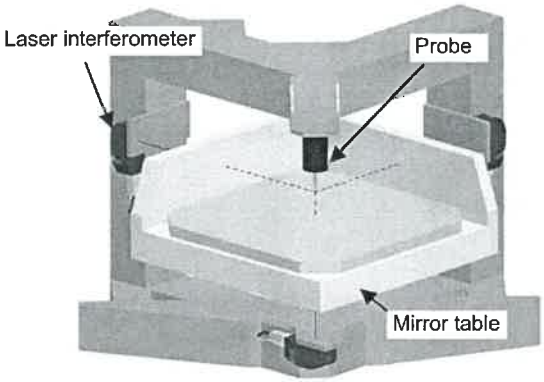

FIGURE 4. 3D Abbe principle.

Rotations of the three translation stages will have no first order influence on the measurements as a result of the fulfillment of the 3D Abbe principle. The influence of the flatness of the three mirrors and the perpendicularity between those mirrors is eliminated by means of a series of on-machine calibration measurements.

Due to the large measuring volume, the Isara 400 must also be capable of measuring parts with high mass. The maximum product load of the Isara 400 is specified at 32.5 kg. In the configuration of the translation axes, a machine concept is chosen in which this (variable) product mass does not need to be moved vertically, see figure 5.

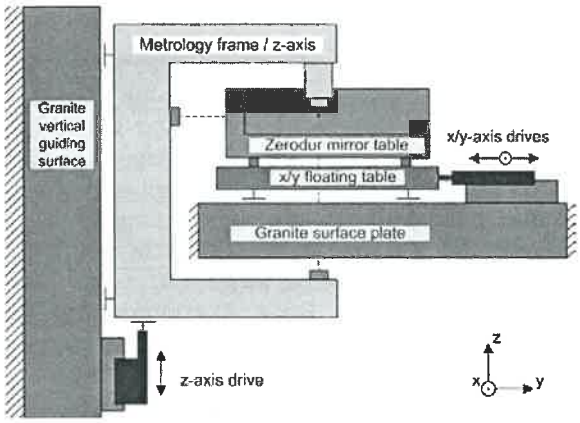

FIGURE 5. Concept of Isara 400.

The product will be placed on the mirror table, which can be moved in X- and Y-direction over a granite plate guided by air bearings. Rather than lifting this table, the complete metrology frame moves in Z-direction, with guiding provided by air bearings placed against a vertical granite guiding surface. This metrology frame contains the three laser interferometers and the probe. All guides are realized with porous media air bearings, enabling frictionless motion. This is especially important for scanning applications, where a contact probe needs to be smoothly dragged along the work piece surface. Isara 400 features several design principles required for precision measurement machines [5]. The design of the most important components will be described in the next sections.

Mirror table

The mirror table assembly is used to support work pieces being measured and it provides three plane mirrors which serve as targets for the laser interferometer. For Isara 400, a monolithic Zerodur mirror table will be used, with three reflective sides.

Because the weight of the product should not influence the flatness and the perpendicularity of the mirrors, an additional product table is used as an interface between the product and the mirror table. This product table is made of Silicon Carbide (SiC), allowing this part to be relatively light and still be very stiff. The supports between the product table and the mirror table feature elastic elements, which allow for differences in thermal expansion between the mirror table and the product table without causing stick-slip in the mounting surfaces.

The three supports of the product table are placed directly above the three supports of the mirror table, so that the weight of the product table including the product is directly led to the supports of the mirror table itself, and no additional deformation of the mirrors occurs. See figure 6 for the design of the mirror table.

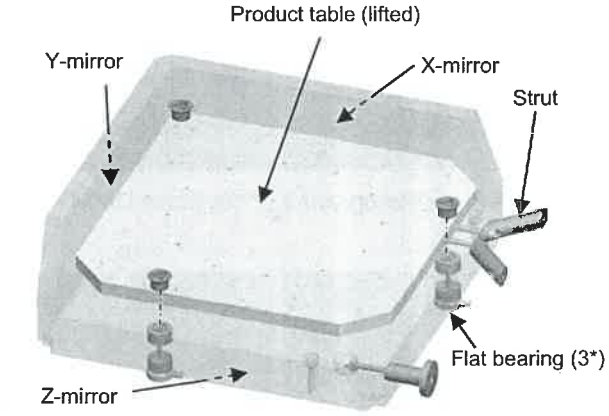

FIGURE 6. Design of X/Y floating mirror table.

The mirror table is supported by three flat air bearings, which fixate the Z position and the Rx

and Ry orientations of the mirror table. The three remaining degrees of freedom are fixed by three lateral struts, which provide the connection between mirror table and the X- and Y-drives. The required preload for the three supporting bearings is provided by the mass of the mirror table assembly with product.

Metrology frame

The metrology frame must hold the three laser interferometers and the measuring probe in a very stable way. This means that it should be very stiff, so that deformations due to acceleration forces are small, but also that its thermal expansion needs to be very low. In addition, as the metrology frame in this design is translated vertically, it is preferable that its mass be as low as possible. The design of the metrology frame is shown in figure 7.

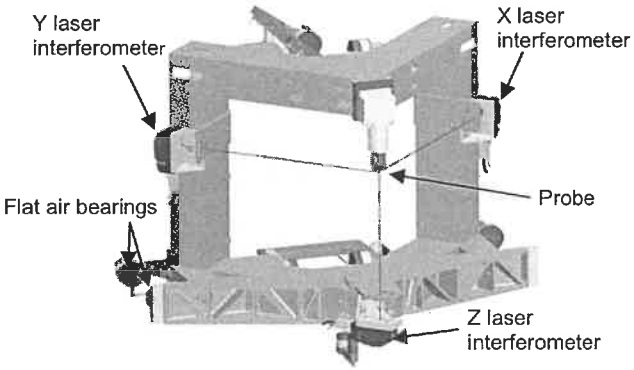

FIGURE 7. Design of the metrology frame.

The metrology frame is made of Silicon Carbide (SiC). Although this material has a larger thermal expansion than for example Invar, it has a much better specific stiffness (ratio of elasticity modulus over density) and better thermal conductivity. The design of the metrology frame is optimized for stiffness, thus allowing the support to be provided by a minimal number of air bearings. The metrology frame is statically determined in six degrees of freedom by means of six flat air bearings mounted on compact elastic cardan joints [6]. All six bearings are preloaded with a flat air bearing on the opposite side. As the machine is a multi probe machine, it contains a kinematic probe interface for an easy exchange of probes.

Drives

The drives are all equipped with linear motors, their own air bearing guides and additional measuring scales for control purposes. These drive units are placed far away from the measuring volume, to minimize the influence of heat generation of the motors.

The X- and Y-drive move the floating table assembly which contains the mirror table. They are positioned on the side of the mirror table, with the X-drive placed on top of a dual Y-drive. The Z-drive moves the metrology frame in vertical direction. It is placed below the metrology frame and connects directly through the centre of mass of this frame. The Z-drive contains an air bearing guide for the linear motor, with an integrated weight compensation system, see figure 8.

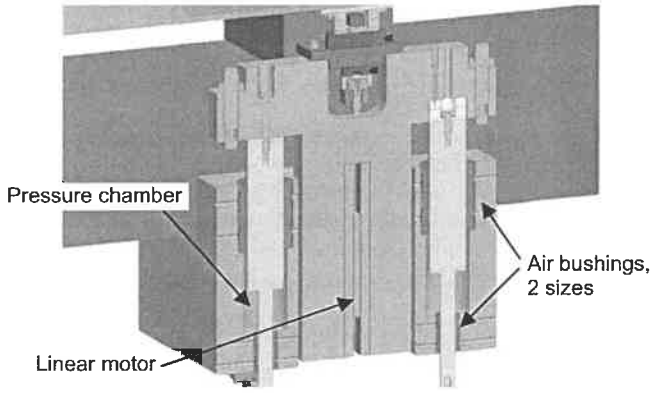

FIGURE 8. Weight compensation system, section view.

This bearing system consists of two shafts; each shaft is guided in two cylindrical air bearings (bushings) with different diameters. At the bottom, the shaft diameter is smaller than at the top. The space between the two bushings is sealed by the two bushings, thus serving as a pressure chamber. This room is supplied with pressurized air, hence creating two air-beared pneumatic cylinders. By supplying exactly the right air pressure, the weight of the metrology frame can be compensated and equilibrium is achieved. As a result, the required force from the linear motor to hold the metrology frame in place is minimized. The heat generation of this drive is therefore very low, as the motor now only needs to provide force for acceleration or deceleration.

ULTRA PRECISION TOUCH PROBE

Introduction

For ultra-precision coordinate metrology, the measuring uncertainty of conventional probe systems is generally too large, for example due to stylus bending. Also, the probing forces may be quite high, making it impossible to measure delicate parts such as optical surfaces. In addition, conventional probes are generally not suitable for measurement of small features, because the probe tip is simply too large. A considerable amount of metrology research, performed over the past 15 years, has been dedicated to the design of new probe systems for ultra-precision coordinate metrology [7,8,9,10]. Many of these designs share a common design feature: the stylus is elastically suspended, allowing deflection of the probe tip and thus reducing probing forces. This deflection is measured by means of an integrated measurement system within the probe.

Design and realization

Building on the previous efforts in the development of ultra-precision touch probes, a new design was realized. See figure 9 for a photo of the realized probe prototype.

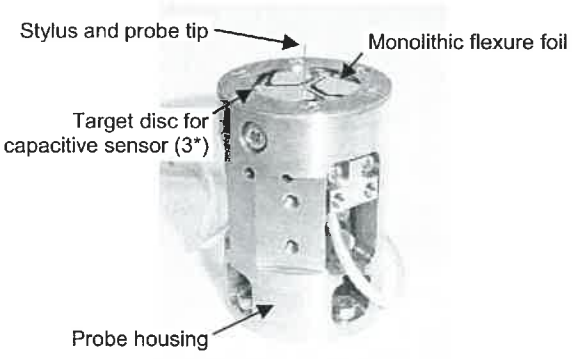

FIGURE 9. Ultra precision touch probe.

The stylus, which consists of a stiff tungsten carbide stylus with a small ruby sphere (Ø0.5 mm) at the end, is again elastically suspended, thus allowing deflection of the tip during probing measurements. The flexure part is a monolithic foil. Three targets for the capacitive probes are implemented in the leaf spring design. The displacements of these targets are measured with capacitive sensors and can be used to determine the X, Y and Z deflections of the probe tip. Except for the sensors, the stylus and the sphere, the complete probe is made out of invar to ensure good thermal stability.

Results

The sensitivity calibration of this probe system is performed on an ultra-precision CMM. The probe is placed in contact with a flat work piece surface, which is located on the product table. The table is then displaced and the output signals of the probe are measured simultaneously with the table displacement, which is measured by laser interferometer systems. By repeating this measurement for multiple probing directions, a full 3D calibration model of the sensitivity is obtained.
This sensitivity calibration is validated by performing additional probing measurements. For one such measurement, up to 5 µm tip deflection, the result is presented in figure 10 (unfiltered data).
For all measurements, the measurement errors are < 10 nm per axis of the coordinate system and 3D measurement errors are < 15 nm.

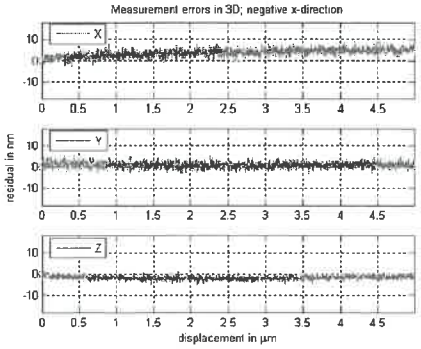

FIGURE 10. Residuals for a probing direction.

MEASURING UNCERTAINTY

An extensive uncertainty analysis was performed to make an accurate estimation of the expected measuring uncertainty of the Isara 400. Some of the most important contributing factors to the total measuring uncertainty are the uncertainty of the laser interferometers, the calibration uncertainty of the mirror table (flatness and perpendicularity), the stability of the metrology frame and the measurement uncertainty of the probe. For all axes, the expected 1D measuring uncertainty is 45 nm (k=2), whereas the full-stroke 3D measuring uncertainty totals 100 nm (k=2), both values are including the described probe system and are valid within the complete measuring volume of the machine.

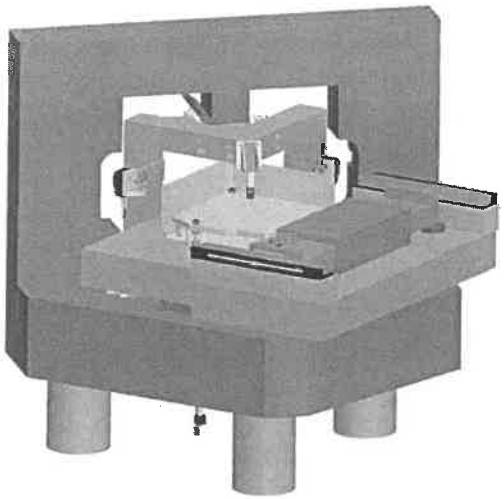

FIGURE 11. Overview of the Isara 400 CMM

CONCLUSION

The new designed Isara 400 CMM is the latest development of IBS Precision Engineering in the coordinate metrology of complex parts with nanometer level measuring uncertainty. The expected 3D measuring uncertainty is 100 nm within the complete measuring volume of 400 x 400 x 100 mm.

Possible applications include the measurements of freeform or complex optics. Also measurements of multiple smaller parts in array setup are possible. To date, no measuring solution combining the precision, measuring volume and multi-probe capability of Isara 400 has been available in the market. Contact probes, such as the presented ultra precision touch probe with capacitive sensors, and also AFM probes can be used. In addition, non-contact probes, such as for example a linnik-interferometer optical probe can be implemented in this machine. Isara 400 is capable of performing scanning measurements as well as point measurements. The presented machine provides a technology basis which can be adapted and optimized for specific user requirements. The machine will be operational before the end of 2009.

The work presented in this document is part of the European projects NanoCMM, sixth framework programme, contract number: FP6-026717-2 and Production4µ sixth framework programme FP6-2004-NI-4.

REFERENCES

[1] Ruijl T.A.M, Ultra Precision Coordinate Measuring Machine – Design, Calibration and Error Compensation, PhD thesis, Delft University of Technology, The Netherlands, 2001.

[2] http://www.zeiss.com/f25

[3] http://www.sios.de/ENGLISCH/PRODUKTE/NMM_E.HTM

[4] Abbe E, Meßapparate für Physiker, Zeitschrift Für Instrumentenkunde, 1890; 10: 446-448.

[5] Schellekens P, Rosielle N, Vermeulen H, Vermeulen M, Wetzels S, Pril W, Design for Precision: Current Status and Trends. Keynote Paper on Precision Engineering & Metrology, Annals of CIRP. 1998; 47/2: 557-586.

[6] Vermeulen J.P.M.B, Ceramic Optical Diamond Turning Machine, design and development, PhD thesis, Eindhoven University of Technology, The Netherlands, 1999.

[7] Peggs G.N, Lewis A.J, Oldfield S, Design of a compact high accuracy CMM, Annals of CIRP. 1999; 48/1 417-420.

[8] Pril, W.O, Development of High Precision Mechanical Probes for Coordinate Measuring Machines, PhD thesis, Eindhoven University of Technology, The Netherlands, 2001

[9] Meli, F, Fracheboud M, Bottinelli S, Bieri M, Thalmann R, Breguet J-M, Clavel R, High-precision, low-force 3D touch probe for measurements on small objects, Euspen international topical conference, Aachen, Germany, May 2003.

[10] Kleine-Besten T, Loheide S, Brand U, Miniaturisierter 3D-Tastsensor für die Metrologie an Mikrostrukturen, Technisches Messen 66, 1999.

SWING ARM OPTICAL CMM

Peng Su, Chang Jin Oh, Robert E. Parks, James H. Burge
College of Optical Sciences
University of Arizona, Tucson, AZ 85721

OVERVIEW

The swing arm profilometer described in reference [1,2] has been a very useful metrology tool for aspheric surface testing. Usually, with previous models of the swing-arm profilometer, axi-symmetric surfaces were measured using mechanical touch probe that limited the accuracy and efficiency of the machine. Recently, we enhanced the swing-arm profilometer with an optical interferometric probe and enhanced the data reduction so that free-form surfaces can be measured. This was demonstrated with the testing of two different 1.4 m off-axis convex parabolic surfaces to an accuracy of about ~5nm rms.

SOC SYSTEM

Basic principle of SOC system

The basic geometry of the Swing-arm Optical CMM (SOC) is shown in Figure 1. A probe is mounted at the end of an arm that swings across the optic under test such that its axis of rotation goes through the center of curvature of the optic. The arc defined by the probe tip trajectory, for a constant probe reading, lies on a spherical surface defined by this center. This is the geometry used for generating spherical surfaces using cup wheels. For measuring aspheric surfaces the probe, that is aligned parallel to the normal to the optical surface, reads only the surface departure from spherical. The SOC uses this simple geometry with an optical, non-contact probe that measures continuous across the optic shown in Figure 2. The swing arm geometry works for convex, concave and plane parts. For measuring concave parts, the scan angle need only be tilted towards the optic, rather than away from the optic as shown for the convex measurements.

The SOC is rigidly mounted to a computer controlled polishing machine to allow *in situ* measurements while the mirror is on the polishing table as shown in Figure 3. The arm length is determined by the size of the test optic. For the off-axis parabola fabricated, a 1.3-m arm

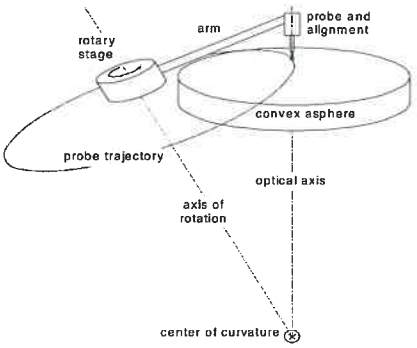

FIGURE 1. Geometry the SOC.

was used. The arm was balanced so it does not exert moments on the frame while it scans. The combination of probe noise, environmental noise, and mechanical instabilities gives a measurement repeatability of about 2 nm rms over a single scan. After calibration of the SOC systematic errors, the measurement error over the full mirror surface is less than 5 nm rms.

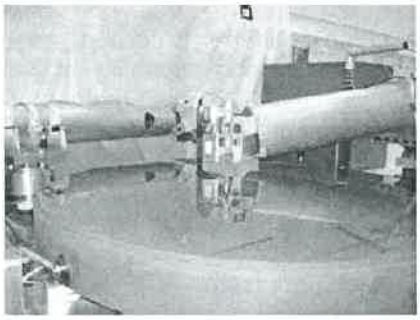

FIGURE 2. SOC measuring a 1.4-m convex off-axis parabolic mirror. Polishing head in back.

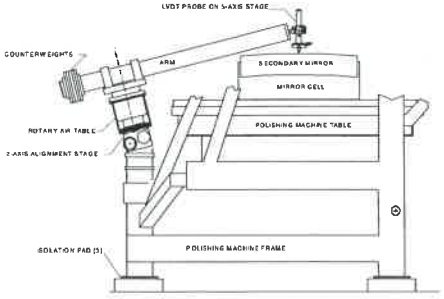

FIGURE 3. Layout of SOC mounted to the polishing machine.

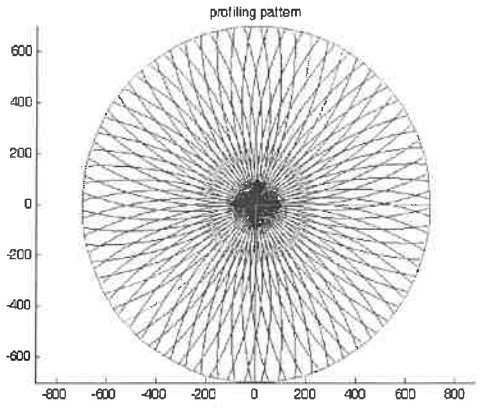

FIGURE 4. SOC profiling pattern

SCANNING METHOD

Fig. 4 shows the profiling pattern we used for testing the 1.4m OAP. Because the sensor remains a constant distance from the center of curvature of the sphere, the sensor has to measure only the departure between the sphere and asphere, in our case about 300 μm total. The sensor makes 64 arcs across the mirror, one arc every 5.625° in azimuth. Since the arcs cross each other at eleven radial positions as the sensor scans the mirror edge to edge, we know the surface heights must be the same at these scan crossings. This crossing height information is used to stitch the scans into a surface. Fig. 5 shows the result of stitching for the ideal shape expected for the OAP.

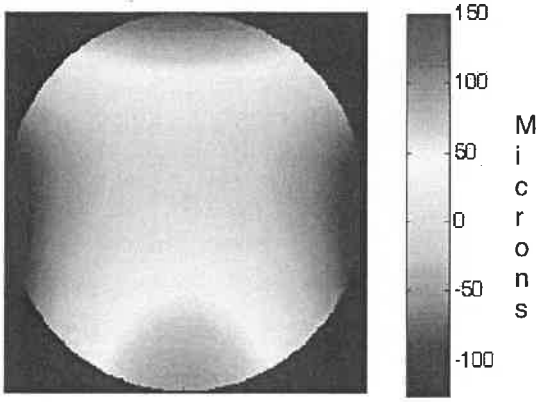

FIGURE 5. Simulated stitching result 51.6um rms

Alignment and calibration of the SOC

SOC system needs to be aligned so that the rotation axis passing through the center curvature of the optic under test to minimize the measurement dynamic range. Also, the probe position relative to the test optic needs to be well known to be able to accurately stitch together the probe data. Given the 1 μm/mm maximum slope change for the OAP, a 10 μm position uncertainty will introduce 10nm of noise into the test data.

Alignment of the SOC

A coordinate system is set up in laser tracker space with the OAP center as the origin and a surface normal at the center as the z-axis. The x-axis joins the parent vertex to the OAP center. There are three laser tracker balls mounted to the probe mount. By rotating the arm and reading out the tracker ball positions, the arm length and rotation axis angle can be calculated in the OAP coordinate system.

The 2-axis stage (elevation and azimuthal) that supports the SOC air bearing is adjusted so that the rotation axis of the SOC passes through the center curvature of the mirror to null tilt and power from the SOC scan. By iteratively scanning the surface and making adjustments, the SOC will be aligned to minimize the probe readout to find a best-fit sphere to the OAP. There is no intrinsic error from the alignment because the software fully removes this. The probe is aligned normal to the surface at the center of the OAP so that the probe will measure the aspheric departure normal to the surface.

Determine probe coordinates

A laser tracker and a PSM [3] are used to calibrate the probe tip coordinates relative to the three tracker balls mounted around it as shown in Figure 6. First the PSM is used to find the reflection from the probe tip, and the three tracker ball coordinates are recorded with laser tracker. After that, the probe is moved away and another tracker ball is put in and adjusted so that the light from the center of the ball is centered on the focus of the PSM. Then the coordinate of this tracker ball is recorded. In this way the coordinate relationship between three mounted tracker balls and the probe tip can be determined. Given the tracker coordinates of the three mounted tracker balls, the coordinates of the probe tip can be calculated. After getting the probe tip and mirror coordinates from the tracker measurements, the measurement positions on the mirror during the scan can be calculated with a simple ray tracing algorithm knowing the mirror parameters.

Instead of using the laser tracker to find the probe tip position during a test, a calibration

between the tip coordinate and the swing arm bearing encoder readout is performed. By rotating the arm, and recording the tip coordinates and encoder readout, a simple fit to a circle can be obtained to define the relationship between the arm encoder data and tip coordinate. During the test only the encoder data and table angle are needed to find the probe tip measurement positions on the mirror.

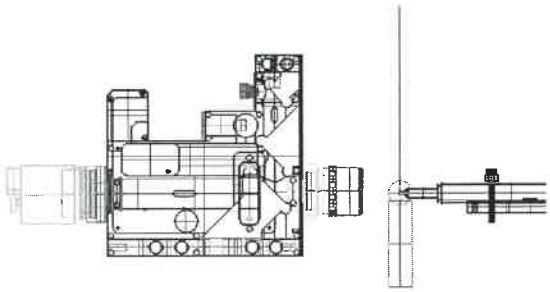

FIGURE 6. Calibrate probe tip coordinates with PSM and laser tracker

Calibration of odd, even errors in the SOC

As with any function, measurement errors in a single scan from SOC system can be divided into odd and even parts. From the scan pattern shown in Figure 4 we know that if all the scan data at different mirror angles are averaged together, odd part due to the mirror will be zero, so the odd part of the average of the scans are totally due to the odd errors in the SOC. Figure 7 (upper) shows an estimate of the odd error in our SOC system (low order linear and cubic terms are removed). Currently, the even errors of SOC system are removed by calibration against full aperture interferometric tests. The full aperture interferometric test used for calibration of the even SOC errors and to act as a comparison with the swing arm profiling is a Fizeau test against a reference sphere located about 6 mm from the OAP. The interferometer is located near the center of curvature of the sphere and the expanding cone of light passes through a hologram and then through the plano polished back of the convex OAP. The reflection from the OAP surface is interfered with the 1st order diffracted beam reflected from the reference sphere to obtain a null interference pattern for a perfect mirror. Figure 7 (lower) shows the calibrated even errors of the SOC system (the quadratic or power term is removed).

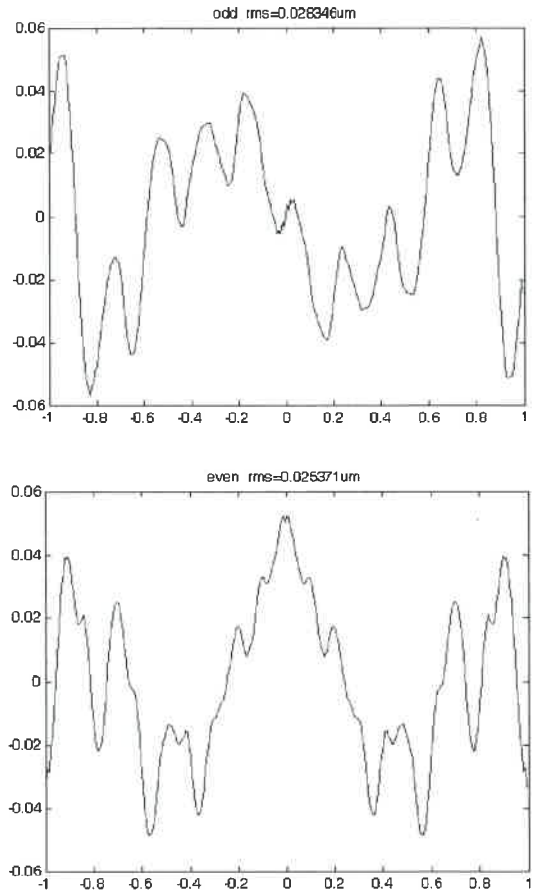

FIGURE 7. (upper) odd errors in the SOC, (lower) even errors. Vertical scale is μm.

For even error calibration, we are planning to add a second probe to the system to obtain the calibration. Since most of the errors of the SOC system are due to the wobble of the arm bearing, we can mount the probes so that they will see the same wobble effect from the bearing and the differential signal from the mirror. By integration, we can recover the mirror data with bearing error removed.

SOC DATA REDEUCTION AND TEST RESULT FOR AN OAP

An off-axis 1.4m convex parabola with 300 um aspheric departure was fabricated using the SOC system as the main method of metrology. During a test, the OAP is scanned in 64 equally spaced arcs. Each arc is scanned 8 times. The data are then stitched together using maximum likelihood algorithm that removes alignment errors [4]. Figure 8(a) shows an example of the raw data from a single scan. Figure 8(b) shows the data with alignment errors removed.

Eight data sets are collected counting forward and backward scans at a single mirror angle during the test. Alignment induced terms are removed from raw data with a least square fit. Figure 8(c) shows the difference of a single forward scan data set from the average of that set of forward scan data; 6 μm rms is the value. Considering a total of eight scans are used for calculating a single mirror angle data set, the data for stitching at different mirror angles would have a noise level of ~2nm.

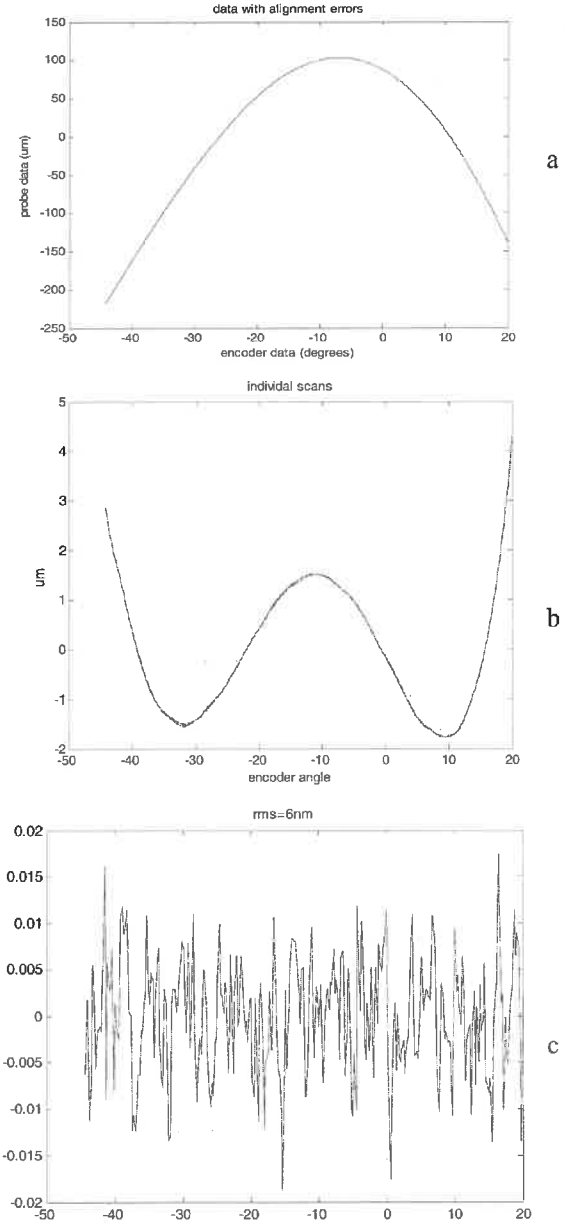

FIGURE 8. (a) Single scan of raw data, (b) scan data with alignment term removed, (c) departure of single scan from mean of data set. Vertical scale is μm.

Surface maps derived from the scan data

The data reduction program produces a surface map which is the departure from the ideal shape of the mirror. Figure 9 shows a comparison of the OAP test results from the SOC and the interferometric null test with astigmatism, coma and trefoil removed from both tests. A direct subtraction of the maps shows a difference ~ 9nm. This data was taken about one week before the OAP was finshed.

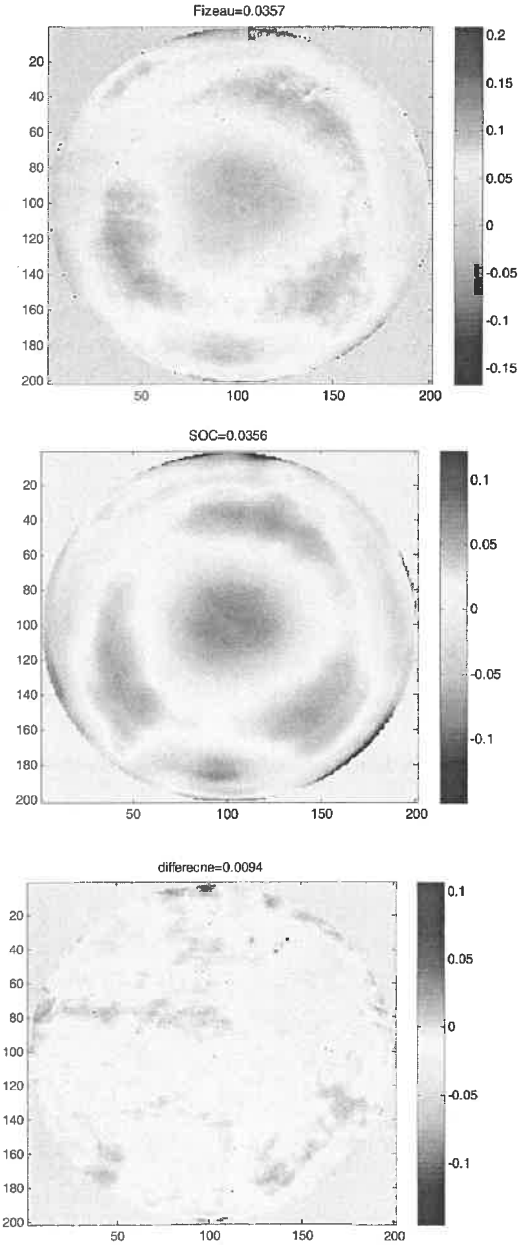

FIGURE 9.. Comparison of the interferometric Fizeau test data (top) and SOC data (middle) with tilt, power, coma and astigmatism removed. The difference (bottom) is 9 μm rms

Fig. 10 shows a comparison of the high frequency information in the same data with the 43 lowest order Zernike terms removed. The difference is ~8nm.

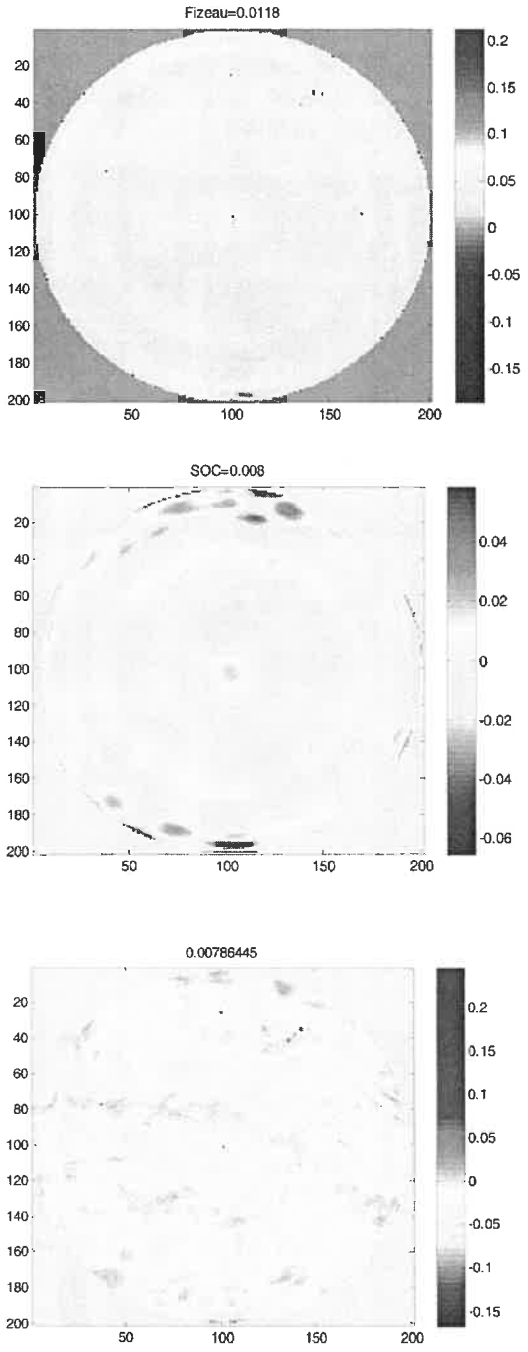

FIGURE 10. Comparison of the interferometric Fizeau test data (top), SOC data (middle) and difference (bottom) with 43 low order Zernike aberration terms removed.

Since there are measurement errors in the interferometric test itself, a second set of data are shown here when the mirror was finished. Fig.11 shows the data with astigmatism, coma and trefoil removed and can be compared directly with Fig. 9. A direct subtraction of the maps shows a difference of ~14nm rms, larger than the week earlier result.

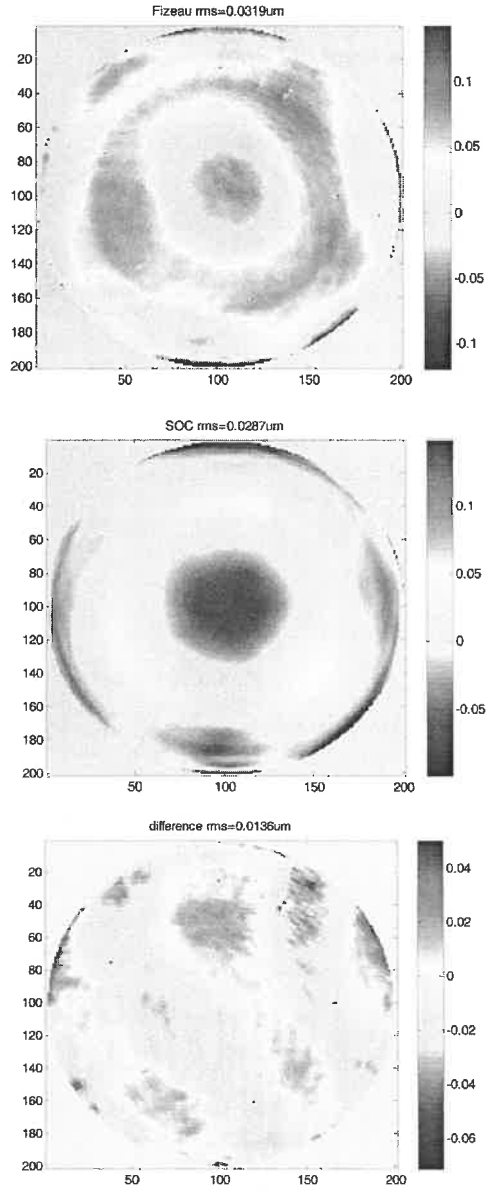

FIGURE 11. Comparison of the interferometric Fizeau test data (top), SOC data (middle) and their difference (bottom) with aberrations up to trefoil removed. While the two sets of test data are better than that taken a week earlier (FIGURE 9) the difference is larger.

However, from a noise analysis of the Fizeau test it is believed the low order differences shown in Fig.11 are mainly from Fizeau test. The difference looks like two fringe print through ghost fringes. Fig. 12 shows the comparison of the high frequency information in the data with the 43 low order Zernike terms removed. The difference is ~5nm rms, better than the difference data from a week earlier. This difference map is dominated by ghost fringes and known errors in the fold flat in the Fizeau test.

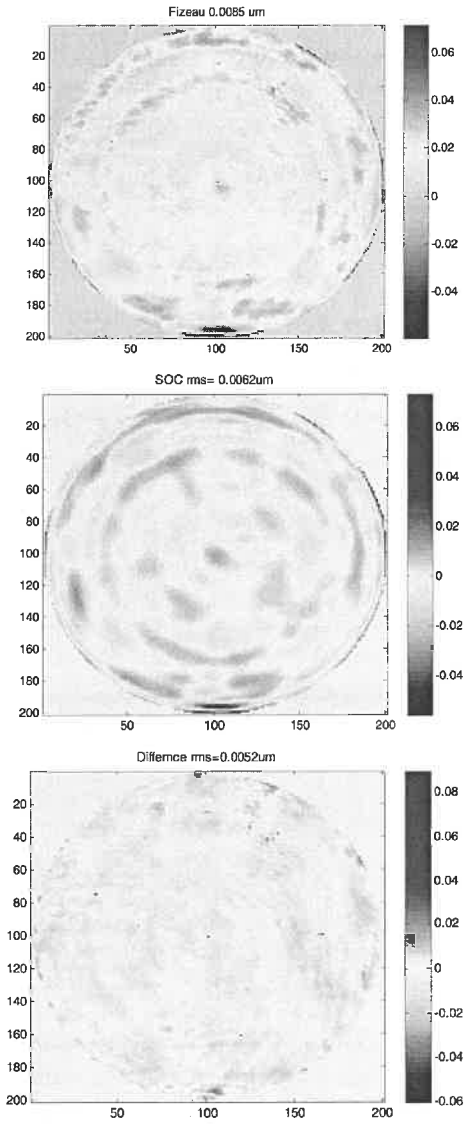

FIGURE 12. Comparison of the final interferometric Fizeau test (top), the final SOC data (middle) and the difference (bottom) with the 43 low order Zernike terms removed.

Given a noise floor for the SOC data of ~2 nm rms as estimated from single scan data and comparisons with the Fizeau data, a ~ 10 nm rms measurement accuracy after the first 10 Zernike terms are removed is a reasonable estimate of the difference between SOC and Fizeau data. After 43 terms are removed, an accuracy of better than 5 nm rms is a reasonable estimate for the difference.

SUMMARY

A profilometer for *in situ* measurement of the topography of aspheric mirrors called the Swing arm Optical CMM (SOC) was built in the Optical Fabrication and Engineering Facility at the College of Optical Sciences, and has been used for measuring the figure of 1.4 m mirrors with a performance rivaling full aperture interferometric tests. The SOC uses a swing arm geometry as a means of supporting a distance measuring interferometric sensor a constant distance from, and pointed along a normal to, the center of curvature of a best fit spherical surface. Thus the sensor measures only the difference between the best fit sphere and the aspheric mirror profile. When the topography of the final mirror figure constructed from 64 profile scans is compared with the full aperture Fizeau test less than 5 nm accuracy is expected.

REFERENCES

[1] Anderson, D.S., Parks, RE., Shao, T., A versatile profilometer for the measurement of aspherics. OF&T Workshop Technical Digest, Monterrey, CA; 1990.

[2] David S. Anderson and James H. Burge, Swing-arm profilometry of aspherics, Proc. SPIE. 2536; 1995; 169-179.

[3] Parks, R. E., Versatile Auto-stigmatic Microscope. Proc. SPIE. 2006; 6290: 62890J.

[4] Peng Su, James H. Burge, Robert A. Sprowl, Jose Sasian. Maximum likelihood estimation as a general method of combining sub-aperture data for interferometric test. Proc. SPIE. 2006; 6342: 63421x-1-63421x-6.

A FEW CASE STUDIES IN UNCERTAINTY USING THE NIST M48 CMM

John Stoup
Precision Engineering Division
National Institute of Standards and Technology
Gaithersburg, Maryland 20899

INTRODUCTION

The Moore M48 coordinate measuring machine (CMM) has provided NIST with unique and very flexible measurement capabilities for many years. Following the move of the machine into the new Advanced Measurement Laboratory (AML) on the Gaithersburg, MD site, the machine's state of the art performance was further improved through rigorous error mapping techniques and improved controls of environmental influences. Expanding on this incomparable measurement ability, the machine has become a platform for attempting unique and non-traditional measurement challenges. These measurements often require special measurement procedures and clever approaches for determining accurate measurement uncertainties of the results. This paper will outline a few of the more recent non-traditional measurements performed with the machine, outline the measurement procedures required for the work, and review how the measurement uncertainty was determined for these results. Included will be measurements of long step gages and ball bar assemblies that far exceeded the measurement volume of the machine, profile measurements of some aspheric and free-form optics with very low measurement uncertainties, and diameter and form measurements of very small sub-millimeter holes using several probe configurations.

NIST M48 CMM

The NIST M48 CMM [1,2] is shown in Figure1. The CMM is currently operated as a three axis machine that can incorporate a rotary fourth axis if required. The motions of the X and Y machine axes (the table and carriage motions, respectively) are accomplished using a precision lead screw coupled with constant force springs on each axis to eliminate backlash motion. The table and carriage motions are restricted using twin V-ways and hundreds of precision cylindrical roller bearings. The machine design takes advantage of the high moving masses of the machine and the mechanical averaging of the bearings to provide extremely smooth and repeatable motion. The Z axis of the machine consists of a ceramic ram and constant force air bearings in a configuration that provides stable translation. The drive motor is decoupled from the RAM by using a threadless nut and flexure

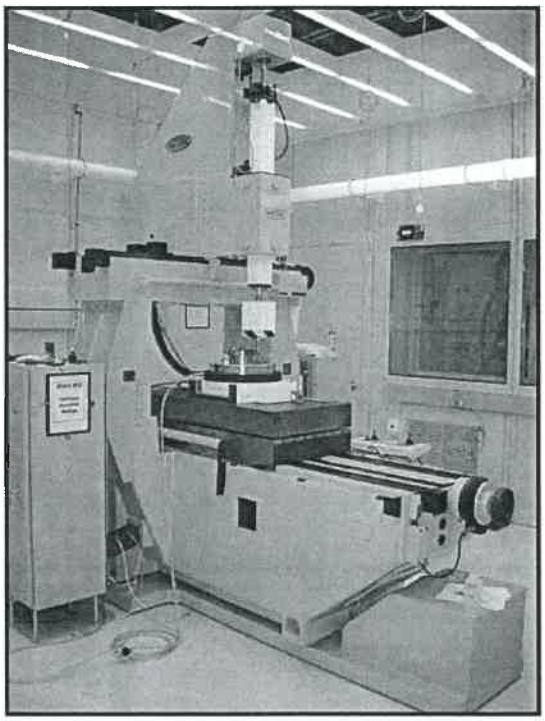

Figure 1. The NIST M48 Coordinate Measuring Machine in the AML Laboratory.

design that minimizes the effects of hysteresis during directional changes.

The standard probe design is an induction type probe and provides short term repeatability as low as 7 nm, as shown in Table 1. The control system of the M48 CMM is designed to require the probe to touch artifact surfaces until a predetermined deflection is reached that corresponds to about a 1.0 Newton (N) applied force. The machine then reverses direction and backs away from the surface slowly, collecting data along the way to extrapolate the result to an undeformed condition. This level of

applied force is routinely used for artifact measurement. The probe does allow for changes to the maximum deflection limits. This feature is valuable for reducing the force exerted on very delicate measurement features or surfaces where applied forces of 1.0 N would deflect or permanently damage the artifact. The repeatability of the collected data is stable in nearly all probing configurations.

MOTION	REPEATABILTY (NM)
X direction (table)	9
Y direction (carriage)	13
Z direction (RAM)	7

Table 1. NIST M48 CMM short term repeatability performance.

The CMM laboratory housed within the AML at NIST is one of the most environmentally controlled laboratories in the world. The thermal environment maintains temperature stability of better than ±0.01˚C over periods of 30 days or more. The relative humidity is also controlled within a range of less than 5% during the same periods of time. This level of environmental control allows NIST to operate the M48 CMM for long periods of time and monitor how the machine behaves independent of most environmental influences.

The measuring volume of the NIST M48 is approximately 1200 mm x 750 mm x 300 mm. The stability of the machine error map and the accuracy of the mapped corrections allow for full use of this volume with no measurable degradation of performance around the periphery edges. The standard artifact measurement procedures are designed to take advantage of the machine stability.

CONTROL STANDARD TECHNIQUES AND UNCERTAINTY DEVELOPMENT

The development of valid control data using an assortment of 1D and 2D artifacts is the most important component of the NIST M48 CMM's uncertainty analysis. Most of the work performed on the M48 consists of measurements of primary artifact standards with very few discrete part measurements. This allows NIST to use classic dimensional artifacts such as ring and plug gages, end standards or gage blocks, spherical standards, 1D step gages, and 2D ball plates and grid plates to quantify the reproducibility performance of the machine as well as the accuracy. Repetitive and redundant measurement of these artifacts over many years have developed very valuable process control parameters that are used to continuously and instantaneously monitor the output of the machine. Figures 2 and 3 are examples of current process control artifact data.

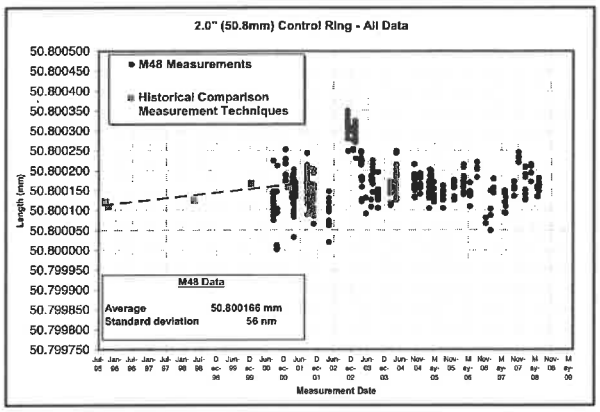

Figure 2. Control chart for an NIST reference ring gage.

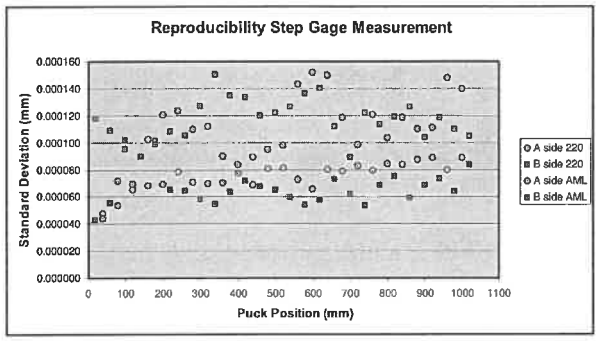

Figure 3. Control chart for the NIST primary 1020 mm step gage.

The measurement uncertainty statements for the NIST M48 are developed by using the standard set of influences that exist for all measuring instruments and the internationally accepted techniques for combining them [3]. The complexity of the CMM measurement uncertainty is reduced by using the control standard data. These provide an estimation of variability from machine influences too multifaceted to control or easily understand. The current 1D measurement uncertainty is calculated as:

$$U\ (k=2) = 0.11\ \mu m + 0.2L\ \mu m \quad (L \text{ is in meters})$$

with a significant portion of the uncertainty coming from the long term performance of the control artifacts. Although the uncertainty budget for the M48 CMM is well established, the measure of non-standard artifacts using measurement protocols with little precedence can prove difficult to characterize. The following sections will outline

several cases where the NIST M48 CMM was used to provide measurements of objects that historically were not performed on the machine due to the difficult nature of the measurement. Intermediate tests of standard artifacts using these non-standard measurement methods will generally be required to provide the appropriate bridge from a comfortable uncertainty analysis to the calculations where long term performance is unavailable. The modifications to the standard measurement uncertainty budget along with the evidence supporting the decisions will be presented along with the changes to the standard measurement protocols.

CASE STUDY 1: 1540 MM STEP GAGE

The longest volumetric dimension limit available on the M48 is about 1200 mm along the X axis of the machine. The measurement of a 1540 mm step gage will require multiple sets of data to be collected to span the full length of the gage and the data stitched together. Fortunately for the M48, the X axis has historically provided the most consistent and reproducible behavior of any directional axis on the machine. The graph in Figure 3 indicates that the long term reproducibility for a 1020 step gage in the AML follows the equation:

$$u_{lt\ reprod} = \pm 0.04\ \mu m + 0.04L\ \mu m \text{ (L is in meters)}$$

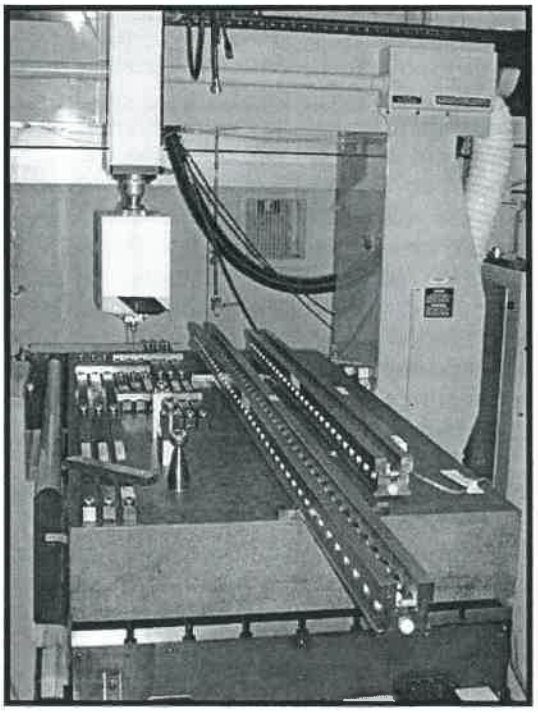

Figure 4. 1540 mm step gage initial setup position.

This is a solid assessment over several years of performance. The challenge will be to duplicate this level of confidence while using a data stitching technique so as not to significantly increase the overall reproducibility term in the error budget when L = 1.5 m. The remaining terms of the standard uncertainty budget will remain the same as long as the fixturing and mounting technique is constant between the two individual setups. The measurement required two artifact mounting setups.

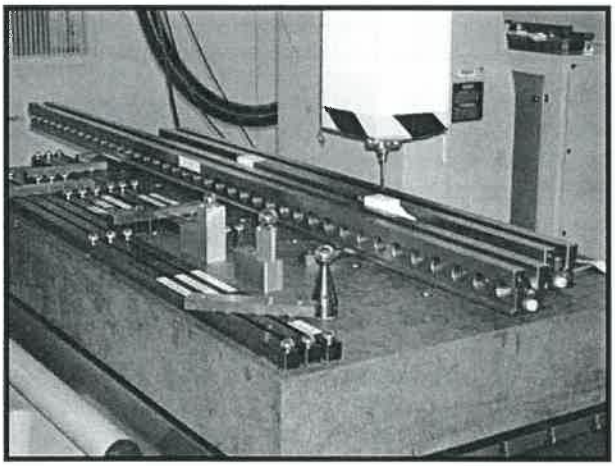

Figure 5. 1540 mm step gage setup position #2.

Figures 4 and 5 show the two measurement setups. The granite surface plate provides just enough length to support the step gage using the Bessel points without having to add additional length to the table surface for mounting. A total of 52 puck steps were measured 5 times in a drift eliminating design. The NIST control step gage was also mounted in a fixed setup along side of the client gage. The NIST gage will act as a bridge to verify that the machine functions including scale and environmental behavior during the two client setups were stable. Analysis of the NIST control step gage repeatability during a single mounting has produced a gage repeatability value of:

$$u_{control\ gage\ repeat\ history} = \pm 0.02\ \mu m + 0.02L\ \mu m$$

The measured control gage performance was similar indicating that the process was consistent with previous performance. The client step gage was moved to the second position and the same measurement program was performed on a duplicate number of puck steps so that the measurement time and thermal environment were similar. The NIST control gage performed similarly. The fact that the NIST control gage was consistent

during both client position measurements provided confidence that the two overlapped measures of the client gage could be combined without needing to increase the standard length dependent uncertainty terms.

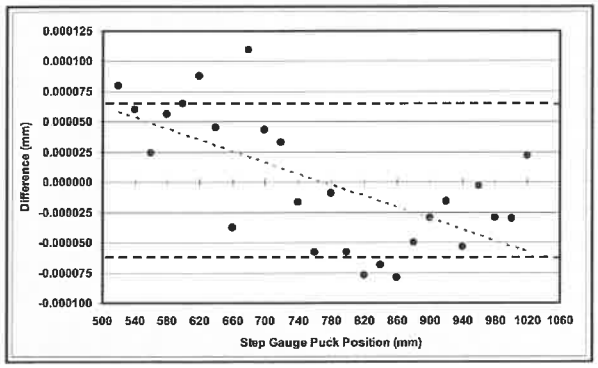

Figure 6. Residual deviations from the two measurements of the overlapped puck steps.

These arrangements produced an overlap of 26 puck steps at the client gage center. The data was combined by calculating the average measurement distance for these repeated puck steps and overlaying the position 2 data set using this offset. The average of the two measurements was calculated and the residual deviations for these overlapped pucks are shown in Figure 6.

CASE STUDY 2: 1600 MM BALL BAR

The measurement of a long ball bar is not trivial. In addition to the sphere geometries and the thermal considerations, the stability of the bar material, the cross sectional shape of the shaft, the straightness of the shaft, and the likelihood of the ball bar being disassembled must be considered. For any high accuracy measurement methods and uncertainty calculations to remain effective, the ball bar must not be disassembled following the measurements. Considering this constraint, the possibility of accidentally bending the long shaft during use or storage is high. Great care must be taken not to change the bar bending behavior as these characteristics dominate the accuracy to which the ball bar length can be measured. Experience with ball bar measurements using the M48 CMM indicates that the longer the ball bar, the less reproducible the center to center length. The rigidity of the shaft becomes the key issue as gravitational forces compel the shaft to sag while being supported by the two spherical ends. Ideally, a perfectly straight shaft of homogeneous material with a perfectly symmetrical cross section would sag consistently independent of the radial orientation of the shaft. All ball bars have bent shafts to some degree, and the sag behavior must be quantified for uncertainty purposes through a set of rotational tests. For ball bars that exceed the measuring volume of the CMM, the bar bending behavior must be determined using a stand alone indicator to directly measure the bar sag at the midpoint of the shaft. Manual axial rotation of the shaft while being supported at the ends easily reveals the extremes of the shaft sag during rotation. Identifying this rotational behavior of the shaft is important for determining the best location to attach a secondary artifact to provide an intermediate and measurable length on the bar.

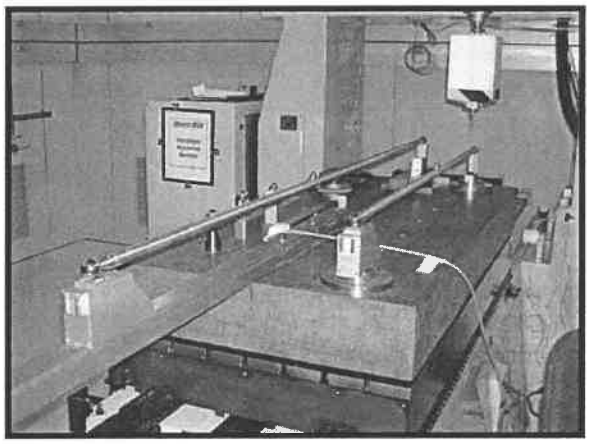

Figure 7. Ball bar sag has significant influence on the artifact length, and the measurement uncertainty, when the shaft is bent. The effect becomes greater as bar length increases.

The ball bar is placed on the CMM table using extensions to carry the sphere supports and to take full advantage of the machine volume, as shown in Figure 7. The mounting assembly is adjusted so the bar is horizontal and aligned with the X axis of the machine. A precision sphere is used as a secondary artifact and is positioned on the shaft using a seating mount and attached using light epoxy. This secondary sphere assembly must be small and light enough not to impart additional sag on the bar, but must be large enough to allow the CMM probe to accurately determine its position as shown in Figure 8. The measurements described here used a 15 mm steel secondary sphere. The ball bar shaft and secondary sphere assembly is probed and rotationally aligned so the sphere is vertically centered on the shaft. This assures the shaft orientation will be reproduced during movements of the ball bar and the probing forces used during the measurement of the secondary sphere will not influence the calculated center position of the sphere in a non-symmetrical way.

in Figure 11 are consistent with the optical flat data discussed earlier. The results appear consistent at a level of 20 nm in both cases. Due to the restricted nature of this measurement and the relatively small size of the test optics, the uncertainty budget is reduced to very few terms and is dominated by this performance dependant effect.

CASE STUDY 4: SUB-MILLIMETER HOLES

The previous measurement studies have all used the same standard Movomatic probe design for data collection. Another area of increasing importance and focus is sub-millimeter features and specifically, internal diameter of sub-millimeter holes. These present true challenges to the standard CMM probe configuration, rendering most of them unusable in all configurations. For internal diameter measurements of sub millimeter holes, the standard probe configuration can not be used for a variety of reasons including operational and mechanical limitations on probe sphere diameter, stem size, and measurement force. For these unique measurement situations, NIST has developed an ultra low force, small diameter fiber-based probe that can be integrated onto the M48 CMM ram and operate as a traditional CMM probe, Figure 12. This probe design [5] is optimized to allow for access into holes as small as 60 μm in diameter and up to 6 mm deep.

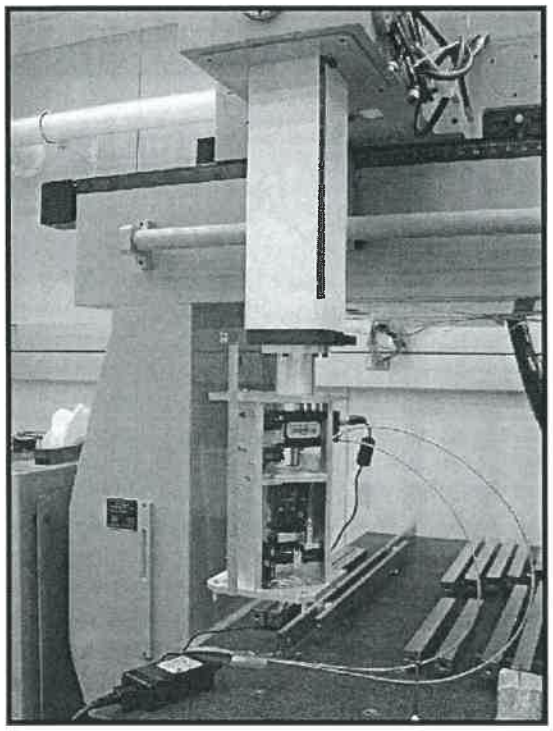

Figure 12. NIST fiber-based probe mounted on the M48 ram.

Figure 13 shows the fiber probe entering a 125 μm diameter ferrule hole. As an example, the measurement of a 125 μm diameter hole is a challenging measurement. The complex interactions of the fiber and imaging components of the probe design are significant and when coupled with variables such as humidity, air currents, and electrostatic charges, can be very unpredictable. One method of addressing these problems is to operate the CMM as a comparator. Mastering artifacts such as small spheres and moderately sized small holes can be characterized to very low uncertainty using other probing systems or direct interferometric methods. These mastering artifacts are used to transfer the accuracy to the micro-sized hole under test and reduce the full knowledge requirements of the complex fiber probe interactions. When used in a comparison process, all that is needed is for the fiber probe to behave consistently during the mastering and data collection measurement cycle.

Although comparative operations can reduce the impact and sensitivity of probe-specific design and correlated behavior, there are still many significant issues that need to be addressed for full confidence in the measured output. Difficult issues such as fiber axis alignment with the artifact axis and residual electrostatic charges are critical as the probe depth increases. Contamination and dirt issues are important due to the extremely small contact forces involved. The cleaning techniques for these very small holes and features have been developed and modified depending on the artifact type and material. The fiber probe tip geometry and size must be verified depending on the data collection procedures and the measurand definition used for the test artifact. Finally, process control data on known artifacts must be developed and studied to determine the repeatability and reproducibility of the

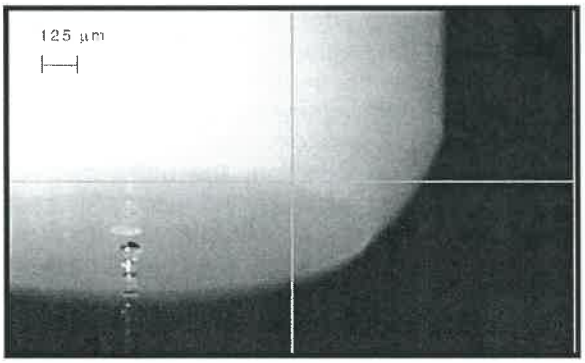

Figure 13. The NIST fiber-based probe entering a 125 μm diameter ferrule hole.

measuring system and the effect of changing actual fiber probe stems. Figure 14 shows a control chart of a 7mm master sphere artifact over a period of several months using multiple fiber stems.

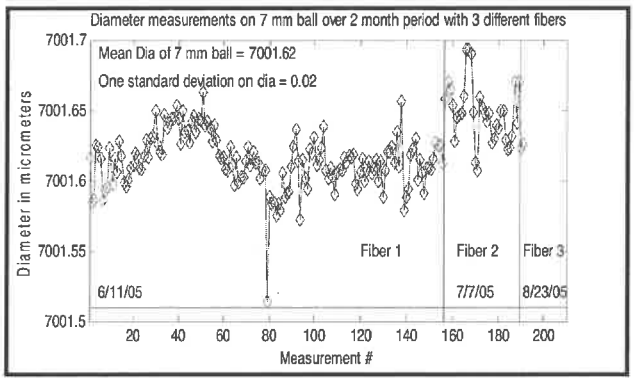

Figure 14. Diameter measurements on the 7 mm master sphere.

UNCERTAINTY BUDGET DEVELOPMENT

The individual components for the M48 uncertainty calculation are shown in Table 3. This budget is the reference for the modifications required by non-typical measurement processes such as those in the previously described case studies. The uncertainty modifications are shown for the previous cases.

M48 Uncertainty Budget 1D/ 2D Measurements

Source	Calculation	µm	ppm
1. Residual Positioning	Multiple rotations of 2D artifacts	0.04	
2. Temperature difference in mapping beam paths	.02°C maximum difference		0.01
3. Laser Frequency Difference	2 x 10-8		0.02
4. Measurement Reproducibility	7 years of data on rings, plugs, step gages	0.04	0.04
5. Edlén Equation	International accepted		0.03
6. Index of Refraction – Air Temp	± 0.006°C beam path accuracy		0.01
7. Index of Refraction - Air Press	± 10 Pascal accuracy		0.04
8. Index of Refraction - Humidity	± 4% accuracy		0.03
9. Temperature Accuracy	0.003°C x 12 µm/m		0.04
10. CTE	0.05°C x 1 µm/m		0.05
11. Contact Deformation	Bi-directional, material	0.002	
12. Gage Surface Geometry	CSY generation error	0.004	

$U(k=2) = 0.11 + 0.20 \times 10^{-6}\ L\ \mu m$
Where L = 1 meter

Table 3. NIST M48 uncertainty budget for 1D artifacts.

Case 1: 1540 mm Step Gage

The uncertainty budget for the 1540 mm step gage is shown in Table 4. The only difference between the standard step gage measurement process and the long 1540 mm gage is the combination of the two individual section measurements. To quantify the additional uncertainty for the overlapping process, several calculations were performed. The data indicated an average difference of 48 nm and the standard deviation of all differences of about 51 nm. Another calculation used the maximum difference (109 nm) in a rectangular distribution and resulted in a standard deviation of 63 nm. We used the most conservative estimate for the budget in Table 4.

M48 Uncertainty Budget: 1540mm Step Gauge

Source	Calculation	µm	ppm
1. Residual Positioning	multiple rotations of 2D artifacts	0.04	
2. Temperature difference in mapping beam paths	.02°C maximum difference		0.01
3. Mapping Laser Frequency Difference	2 x 10-8		0.02
4. Measurement Reproducibility	7 years of data on rings, plugs, step gages	0.04	0.04
5. Edlén Equation	International accepted		0.03
6. Index of Refraction – Air Temp	± 0.006°C beam path accuracy		0.01
7. Index of Refraction - Air Press	± 10 Pascal accuracy		0.04
8. Index of Refraction – Humidity	± 4% accuracy		0.03
9. Temperature Accuracy	0.003°C x 12 µm/m		0.04
10. CTE	0.05°C x 1 µm/m		0.05
11. Contact Deformation	Bi-directional, material	0.002	
12. Gage Surface Geometry	CSY generation error	0.004	
13. Bi-direction Overlap Fitting	experimental data estimate	0.063	

$U(k=2) = 0.17 + 0.20 \times 10^{-6}\ L\ \mu m$ Where L = 1 meter

Table 4. Uncertainty budget for the 1540 mm step gage measurements. The only change to the standard budget is the additional term for the bidirectional overlapped fitting from the experimental data.

Case 2: 1600 mm Ball Bar Measurement

The uncertainty budget for the 1600 mm ball bar is shown in Table 5. The standard M48 uncertainty components all apply in addition to two extra terms. The first is based on the experimental test data for the accuracy of the secondary sphere technique used to produce a pivot point for the ball bar end to end rotation. The technique was used on two standard length ball bars and produced a relatively consistent bias that indicated some possible dependence on length. An estimate of a + 1.0 μm bias with an uncertainty of ± 0.5 μm was used. The second extra term is based on the effects of gravitational sag on the ball bar shaft. The shaft cannot be perfectly straight, inducing a sagging effect that changes the ball bar length as the shaft is axially rotated. The data indicated a range of 7.2 μm during the axial rotation. This leads to the bending term in the itemized budget. It is noted that at these ball bar lengths, the artifact sagging behavior is the dominant uncertainty source, dwarfing the instrument terms as well as the technique term.

M48 Uncertainty Budget: 1600mm Ball Bar

Source	Calculation	µm	ppm
1. Residual Positioning	Multiple rotations of 2D artifacts	0.04	
2. Temperature difference in mapping beam paths	.02°C maximum difference		0.01
3. Mapping Laser Frequency Difference	2 x 10-8		0.02
4. Measurement Reproducibility	7 years of data on rings, plugs, step gages	0.04	0.04
5. Edlén Equation	International accepted		0.03
6. Index of Refraction – Air Temp	± 0.006°C beam path accuracy		0.01
7. Index of Refraction - Air Press	± 10 Pascal accuracy		0.04
8. Index of Refraction – Humidity	± 4% accuracy		0.03
9. Temperature Accuracy	0.003°C x 12 µm/m		0.04
10. CTE	0.05°C x 1 µm/m		0.05
11. Contact Deformation	Bi-directional, material	0.002	
12. Gage Surface Geometry	CSY generation error	0.004	
13. Secondary Ball Technique	~1µm bias ±0.5um estimate	0.5	
14. Ball Bar Bending	½ experimental range/1.73	2.1	

$U(k=2) = 4.36 + 0.20 \times 10^{-6}\ L\ \mu m$ or 4.68 µm

Table 5. Uncertainty budget for the 1600 mm ball bar measurements.

Case 3: Freeform Surfaces

The uncertainty budget for the freeform surface measurements is shown in Table 6. The length dependent, the elastic deformation, and the reproducibility terms based on historical artifact data are negligible due to the limited nature of the surface measurement and the change in the measurement

M48 Uncertainty Budget: Freeform Surface Geometry

Source	Calculation	µm	ppm
1. Residual Positioning	Multiple rotations of 2D artifacts	neg.	
2. Temperature difference in mapping beam paths	.02°C maximum difference		0.01
3. Mapping Laser Frequency Difference	2 x 10-8		0.02
4. Measurement Reproducibility	7 years of data on rings, plugs, step gages	0.04	0.04
5. Edlén Equation	International accepted		0.03
6. Index of Refraction – Air Temp	± 0.006°C beam path accuracy		0.01
7. Index of Refraction - Air Press	± 10 Pascal accuracy		0.04
8. Index of Refraction – Humidity	± 4% accuracy		0.03
9. Temperature Accuracy	0.003°C x 12 µm/m		0.04
10. CTE	0.05°C x 1 µm/m		0.05
11. Contact Deformation	Bi-directional, material	0.002	
12. Gage Surface Geometry	dev from normal (aspheric)	~ 0.010	
13. Reversal Reproducibility	experimental 25nm/1.732	~ 0.015	

$U(k=2) = 0.036$ µm

Table 6. Uncertainty budget for freeform surface measurements.

procedure to a reversal technique. This technique along with the measurements of known optical flat and parabolic surfaces yields a more relevant reproducibility uncertainty of about 15 nm. Another term is added for potential approach vector deviations on parabolic surfaces and the subsequent impact the probe sphere diameter has on the actual contact location. This term is correlated to the probe sphere diameter used and can be reduced by using small diameter probes.

Case 4: Sub-Millimeter Holes

The uncertainty budget for sub-millimeter hole measurements is shown in Table 7. The budget is different in that the length dependent terms are negligible for very small feature measurements.

M48 Uncertainty Budget: Microholes w/Fiber Probe

Source	Calculation	µm	ppm
1. Residual Positioning	Multiple rotations of 2D artifacts	~ 0.02	
2. Temperature difference in mapping beam paths	.02°C maximum difference		0.01
3. Mapping Laser Frequency Difference	2 x 10-8		0.02
4. Measurement Reproducibility	7 years of data on rings, plugs, step gages	0.04	0.04
5. Edlén Equation	International accepted		0.03
6. Index of Refraction – Air Temp	± 0.006°C beam path accuracy		0.01
7. Index of Refraction - Air Press	± 10 Pascal accuracy		0.04
8. Index of Refraction – Humidity	± 4% accuracy		0.03
9. Temperature Accuracy	0.003°C x 12 µm/m		0.04
10. Coefficient of Thermal Expansion	0.05°C x 1 µm/m		0.05
11. Uncertainty of Master Spheres	Interferometry	0.008	
12. Contact Deformation	Bi-directional, material	neg.	
13. CSY Alignment & Geometry	CSY generation error	0.020	
14. Fiber probe Reproducibility	Experimental data	0.025	

$U(k=2) = 0.076$ µm

Table 7. Uncertainty budget for fiber based probe small hole measurements.

The elastic deformation and the reproducibility terms are replaced due to the high correlation to the mechanical operation of the probe being used. The deformation is negligible due to the tiny forces applied, and the reproducibility term is replaced with results from artifact measurements using various fiber stems. The probe has been demonstrated to perform at a level of about 25 nm.

Two additional uncertainty terms are also added to the budget. The first is related to the variability in the determination of the artifact coordinate system. Coordinate system generation and alignment for these very small features is sensitive to the actual data collection and the locations of surface sampling. Artifact results can vary small amounts by simply changing the scheme and locations for collecting coordinate system data. The second term results from the fact that the CMM is operated as a direct comparator using known spherical artifacts. The uncertainty of the master spheres is included in the budget. The interferometric technique used for the master sphere diameter calibration has very low uncertainty and contributes only slightly to the overall fiber probe error budget.

REFERENCES

[1] Trade names and company products mentioned in the text does not imply recommendation or endorsement by the National Institute of Standards and Technology.

[2] Stoup, J. R., Doiron, T. D., The Accuracy and Versatility of the NIST M48 Coordinate Measuring Machine. SPIE - Recent Developments in Traceable Dimensional Measurements. 2001; 4401: 136-146.

[3] Guide to the Expression of Uncertainty in Measurement. 1st Edition, International Organization for Standardization (ISO), Switzerland: 1993.

[4] Machkour-Deshayes, N., Stoup, J. R., Lu, J., Soons, J. A., Griesmann, U., Polvani, R. S., Form-Profiling of Optics Using the Geometry Measuring Machine and NIST M-48 CMM. Journal of Research, National Institute of Standards and Technology. 2006; 111: 373-384.

[5] Muralikrishnan, B., Stone, J. A., Stoup, J. R., Fiber Deflection Probe for Small Hole Metrology. Journal International Societies for Precision Engineering and Nanotechnology. 2006; 30: 154-164.

MEASUREMENT OF TRUE POSITION OF THREADED HOLES

Edwin A. Bryce
Mechanical Measurements Department
Sandia National Laboratories
Albuquerque, New Mexico, USA

INTRODUCTION

The use of threaded holes for fastener applications is common place in manufacturing. The location and orientation of the threaded hole is crucial in assuring that the fastener is properly engaged, so that failure of the fastener does not occur. However, measurement of the threaded hole "true position" is something that is taken for granted by many in industry. Often the techniques used make incorrect assumptions and or take shortcuts to save time and money.

Related Reference for Threaded Holes

Tolerances for threaded holes using the principles stated in the American Society of Mechanical Engineers (ASME) Y14.5M-1994 "Dimensioning and Tolerancing" preferably use the positional tolerancing method (Section 2.1.1.1). Section 2.9 of the standard states "Each tolerance of orientation or position and datum reference specified for a screw thread applies to the axis of the thread derived from the pitch cylinder." If required the tolerance can be specified to either the major or minor diameter of the thread, however the default condition is the pitch cylinder.

Motivation for Interest in Issue

Interest in the techniques used and the results obtained came about when the measurement of threaded holes on a cylinder surface was required (See Figure 1). In this example the location of the threaded holes was determined using threaded location gages.

The use of these gages is common in dimensional metrology when using coordinate measuring machines (CMM) to determine position. There are various manufactures of these gages and designs vary. Basically the gages are made up of a cylindrical section, of known size and form, which is co-axial to the pitch cylinder axis of the threaded section. The standard gage has a seating face which is perpendicular to the pitch cylinder axis. When inserted into the threaded hole the cylindrical section is probed to establish the axis of the cylinder which in turn establishes the pitch cylinder axis. Using CMM software the position of the hole over the entire length of the feature is determined.

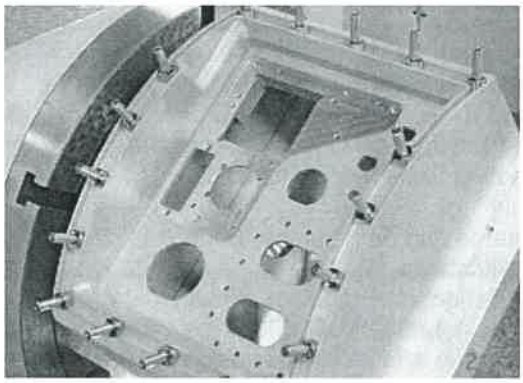

Figure 1. Threaded holes on a curved surface

PROBLEM

The standard threaded location gage when fully engaged contacts the part surface at the seating face. Because the seating face is perpendicular to the pitch axis, on a nominally flat surface, one might not see any apparent problem, but in the case of a curved surface only "line contact" is made which allows for the gage to rotate or rock (see Figure 2).

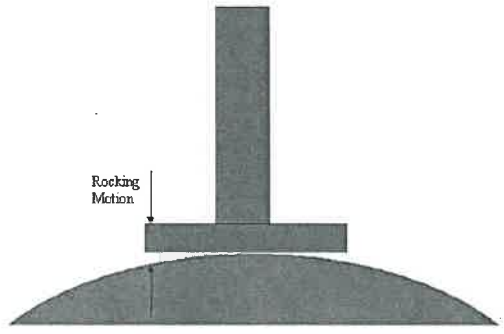

Figure 1. Rocking motion of device

The mating surface of the threaded location gage should not influence the position or orientation of the cylindrical feature. A measurement technique is needed that is not influenced by the gage seat or the part surface.

APPROACH

Evaluation of various threaded location gages was made along with evaluation of a position determination technique in which the thread form itself is probed by the CMM.

Threaded Location Gages

A survey of commercially available products was made and four various designs were acquired for testing. The first gage (See Figure 3) is a standard threaded gage. The second gage (See Figure 4) has a thread form which has been cut to allow expansion of the threaded portion. This expansion provides constant compliance with the thread form and there is no contact of a seating face. The third gage (See Figure 5) utilizes a tapered thread form similar to a standard pipe thread. When inserted into the threaded hole the gage is rotated until compliance is felt. The last gage (See Figure 6) is a rather unique in that a series of six balls located on the thread form are pushed outward to make contact with the flank of the thread form. The manufacturer has determined that the contact point on the flank is at the pitch cylinder of the thread. Once the balls are engaged the gage is aligned and ready for the CMM measurement.

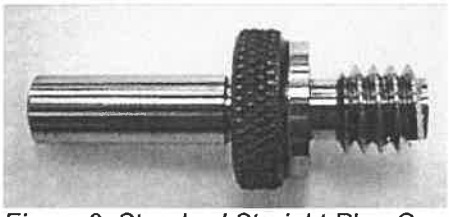

Figure 2. Standard Straight Plug Gage

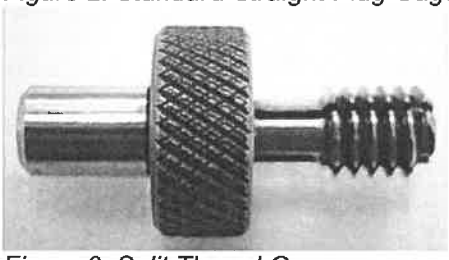

Figure 3. Split Thread Gage

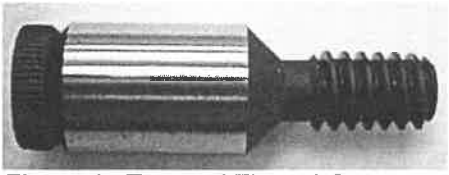

Figure 4. Tapered Thread Gage

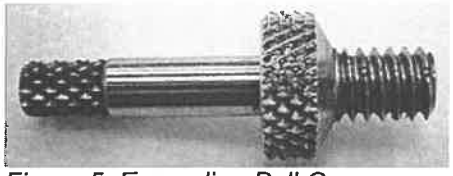

Figure 5. Expanding-Ball Gage

Thread Form Probing

The final technique evaluated was to directly probe the thread form. This technique is used by many in industry to avoid the cost and time involved when using the threaded location gages. Direct probing of the threaded hole is performed using a helical path. This helical path is determined using the lead (linear distance traveled in one rotation of the fastener) of the thread. This method will insure that all the CMM probing points are made at the same location on the thread form, although not necessarily on the pitch cylinder (See Figure 7).

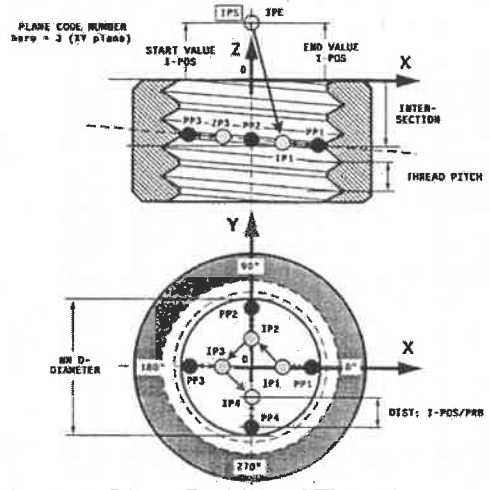

Figure 6. Direct Probing of Thread

Test Pieces

Suitable test pieces were fabricated to use in evaluation of the gages and techniques. For the purposes of this project a thread size of ¼"-20 UNC-2B was selected, as this is a common fastener size used in industry. The first test piece was made of steel and the thread form was lapped to produce a gage quality surface (See Figure 8). The top surface (datum A) and outside diameter (datum B) were ground surfaces. The second test piece was fabricated from aluminum and the threaded hole was formed using a standard tapping operation (See Figure 9). The remainder of the part was turned using a conventional lathe. Both test pieces had a through hole located near the outer edge of

the part which would serve as a tertiary datum C.

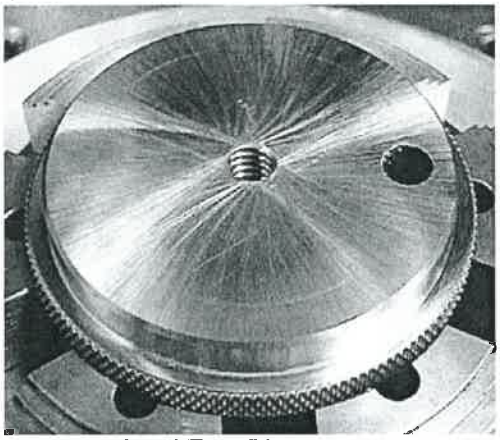

Figure 7. Steel Test Piece

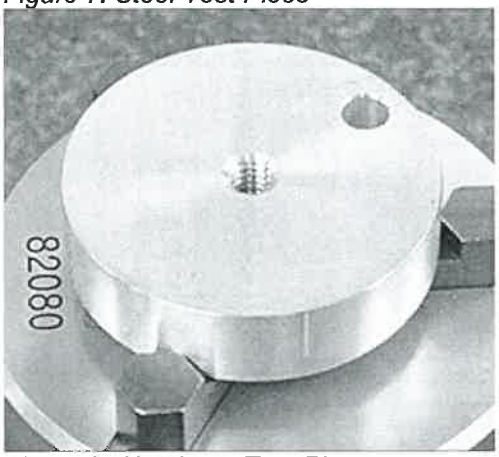

Figure 8. Aluminum Test Piece

Evaluation Procedure

Thread Location Gages

A datum reference frame (DRF) was established using the top surface, outside diameter and through hole. Each threaded location gage was inserted into the test piece and the CMM was programmed to take a total of thirty two points (eight equally spaced points at four different levels) over the length of the cylinder portion of the gage. Due to the short length of the split thread gage a total of twenty four points (eight equally spaced points at three levels) were taken. The measured cylinder axis was used for evaluation.

Direct Probing of Thread

The CMM program measured two circles (8 equally spaced points) at both ends of threaded hole. A line was constructed through the centers of both circles to serve as the axis in evaluation.

Data Collection

The CMM part program was executed a total of ten times for each test piece on three different CMM's, each of different accuracy. The thread location gage was removed between each run and the DRF was re-established with each run. The test piece was not removed from the fixture between runs. The typical setup for the tests is shown in Figure 10.

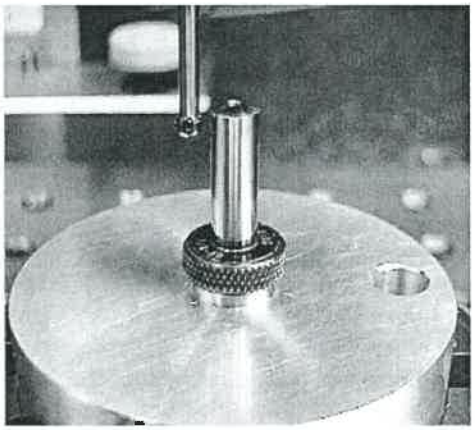

Figure 9. Typical CMM Run

The CMM evaluated the position of the threaded hole over the length of the feature. The length was from Datum A (Z zero) to -0.5 inches (thickness of test piece). The difference in the two Z axis locations is an indication of the tilt or orientation of the threaded hole axis.

RESULTS

Results for the steel test piece are listed in Table 1 and in Table 2 for the aluminum test piece. The results listed for Z = 0.0 inches (Datum A) and Z -0.5 inches include deviations in the X and Y axes, standard deviation of the data set and the true position result (TP).

A complete uncertainty analysis will be provided during the presentation and in the full paper submitted.

Assumptions

An initial assumption was made that the test results would show a significant range of results between the gages and between the gages and the direct probing method. This was not proven in the results, although the range was greater between the gages and the direct probing method. For the steel test piece the TP range for the gages was 0.0003 inches and for the aluminum test piece the TP range was 0.0006 inches. The TP range between the gages and

the direct thread probing was 0.0015 inches for the steel test piece and 0.0024 inches for the aluminum test piece.

CONCLUSION

Initial indications were that the surface of the threaded hole would influence the range of results. However these tests used a nominally flat surface as Datum A and this fact may have influenced the test results. Although the difference between the gages and the direct probing method are slightly greater, one would need to evaluate if the results justify the cost of the gage. The savings in time spent for insertion of the gage and the gage cost could make direct probing a preferred method.

This project has motivated efforts to conduct further tests to address the issues with threaded holes to yield a minimal uncertainty.

ACKNOWLEDGEMENTS

Sandia is a multiprogram laboratory operated by Sandia Corporation, a Lockheed Martin Company, for the United States Department of Energy's National Nuclear Security Administration under Contract DE-AC04-94AL85000.

TABLE 1. Average of All CMM's – Steel Test Piece (Results in Inches)

		Datum A - Z Axis Zero			Projected -0.5 inches Z Axis		
	Axis	Deviation	Std. Dev.	TP Result	Deviation	Std. Dev.	TP Result
Standard Straight Gage	X	-0.00011	0.00002	0.0003	-0.00017	0.00003	0.0005
	Y	-0.00011	0.00001		-0.00017	0.00006	
Split Gage	X	-0.00016	0.00002	0.0003	0.00029	0.00037	0.0006
	Y	-0.00001	0.00002		-0.00011	0.00007	
Tapered Gage	X	-0.00017	0.00013	0.0004	-0.00029	0.00007	0.0009
	Y	-0.00010	0.00007		-0.00037	0.00030	
Expanding Ball Gage	X	0.00004	0.00002	0.0004	0.00029	0.00021	0.0006
	Y	-0.00019	0.00005		-0.00001	0.00021	
Direct Thread Probing	X	0.00043	0.00103	0.0009	0.00094	0.00059	0.0020
	Y	-0.00017	0.00001		0.00034	0.00045	

TABLE 2. Average of All CMM's – Aluminum Test Piece (Results in Inches)

		Datum A - Z Axis Zero			Projected -0.5 inches Z Axis		
	Axis	Deviation	Std. Dev.	TP Result	Deviation	Std. Dev.	TP Result
Standard Straight Gage	X	-0.00082	0.00002	0.0027	-0.00088	0.00007	0.0033
	Y	0.00110	0.00002		0.00141	0.00063	
Split Gage	X	-0.00018	0.00004	0.0027	-0.00061	0.00039	0.0031
	Y	0.00132	0.00005		0.00140	0.00010	
Tapered Gage	X	-0.00047	0.00004	0.0024	-0.00106	0.00053	0.0031
	Y	0.00113	0.00018		0.00112	0.00019	
Expanding Ball Gage	X	0.00029	0.00016	0.0024	-0.00061	0.00087	0.0027
	Y	0.00117	0.00006		0.00120	0.00016	
Direct Thread Probing	X	0.00080	0.00005	0.0016	0.00002	0.00064	0.0003
	Y	0.00004	0.00010		0.00014	0.00015	

UNCERTAINTY IN TORQUE CALIBRATION

Theodore D. Doiron
National Institute of Standards and Technology
Dimensional Metrology Group
Gaithersburg, MD 20899-8211, USA

The primary method of calibrating torque standards in industry uses weights, gravity and a well characterized torque arm.

The uncertainty of a simple case is presented, and the limits of standard laboratory practice are discussed.

NCSLI BOARD OF DIRECTORS MEETING HIGHLIGHTS

Roger N. Burton
Honeywell, FM&T / KC
Kansas City, MO 64141-6159 USA

This presentation will provide an overview of the recent NCSLI Board of Directors meeting held in San Diego, CA in January 2009. Topics to be covered include a summary of the 2008 conference, notification of the 2009 conference to be held July 26-30, 2009 in San Antonio, TX, award and scholarship information, new and revised publications and documents, NIST international news, World Metrology Day planned for May 20, 2009, Learning & Development activities, upcoming training events at the Boulder facility, future BOD meeting dates, and opportunities for people to become involved and lend their expertise and support to any of the NCSLI committees.

TEST UNCERTAINTY IN ISO TC213

Edward P. Morse, Samira A. Khanam
Center for Precision Metrology
University of North Carolina at Charlotte
Charlotte, NC, USA

ABSTRACT
This paper will provide a short report of the current status of "test uncertainty" in Technical Committee 213 (Dimensional and geometrical product specifications and verification – e.g., tolerancing and metrology). This idea has powerful implications in the buying and selling of metrology equipment, and in equipment calibration. We have all become familiar with the idea of measurement uncertainty, and many of us have developed uncertainty budgets for various measurements and measurement processes.

Test Uncertainty is, however, a horse of a different color. Test uncertainty is the uncertainty for which the "tester" is responsible when evaluating an instrument. Contributors to the test uncertainty may include the uncertainty of the reference artifact used by the tester and details of the tester's measurement procedure that result in errors and uncertainty. Most notably absent from the test uncertainty is the repeatability and resolution of the instrument under test.

To help with understanding this Test Uncertainty, this paper will discuss the motivation of its use, which is driven in large part by the use of the default decision rule outlined in ISO 14253-1. The paper will then look at two different methods for understanding test uncertainty: first, through the differentiation of the contributors for which the tester is responsible, and second, through the search for, and examination of, the measurand for which the uncertainty is the test uncertainty – recall that uncertainty is always associated with a measurand. Finally, we will discuss some work performed in attempting to evaluate test uncertainty, and describe future directions that may quantify test uncertainty through testing.

BACKGROUND
ISO 14253-1 provided a default decision rule for the impact of uncertainty on whether a workpiece can be considered conforming to specifications. The choice of words within the document is unfortunate, however, in that it puts the decision in the context of 'proving' conformance or non-conformance. However, the essence of the default rule is that, for conformance to be 'proved,' the measured value must lie within the specification limits by at least the expanded uncertainty of the measurand. Conversely, 'proving' that a measurand is non-conforming requires that the measured value be outside of the specification limits by at least the expanded uncertainty of measurement. A more complete document on decision rules, which better recognizes the business aspects of these decisions, is ASME B89.7.3.1.

ISO standards for the specification of CMM performance that followed the release of ISO 14253-1 refer to this document and its default decision rule in assessing whether the CMM satisfies its performance specification. For example, from ISO 10360-2:2001, we have: *The performance of the CMM used for measuring size is verified if the error of indication of a CMM for size measurements, E, is not greater than the maximum permissible error of indication of a CMM for size measurements, MPE_E, as specified by the manufacturer and taking into account the uncertainty of measurement according to ISO 14253-1.* The key wording to notice in the text above is *the uncertainty of measurement.* If we believe this to be measurement uncertainty, this statement has the unintended consequence of essentially doubling the MPE values that manufacturers must state in order to 'prove' conformance to their CMM specification.

For example, if the CMM manufacturer believes that the error in measuring a certain reference length anywhere within the CMM volume will not

exceed 10μm, it seems reasonable that the MPE for length measurement would be 10μm. However, the uncertainty of measurement (thought of in the normal way – as measurement uncertainty) is also 10μm, so the MPE would have to be increased to 20μm. This is because the manufacturer is required to provide a test result (the E value) that is at least 10μm less than the MPE in order to 'prove' conformance.

INITIAL WORK

The impracticality of specifying these inflated MPE values was immediately recognized by the CMM working group (WG10) within TC213, but there was still a desire to comply with the default rule of 14253-1. The natural solution seemed to lie with redefining the uncertainty that was used to create the guard band in the decision rule.

The development of TS 23165:2006 was based on the definition and quantification of Test Uncertainty for CMM testing. Test Uncertainty is defined in this document as the *expanded uncertainty U, associated solely with the testing equipment and its use in the test, which modifies the conformance and non-conformance zones, according to the decision rule in ISO 14253-1.* The important part of this definition is that only the uncertainty contributors associated with the test equipment and its use are counted towards the test uncertainty. This is a reasonable strategy, as the uncertainty associated with the measuring instrument (i.e. by determining errors in measuring a calibrated artifact) is what we wish to test, and it is the uncertainty in our ability to reveal these errors that determines how well we can say that a CMM does or does not meet its specification.

The 23165 document explicitly examines the contributors to test uncertainty for the two main tests in the ISO 10360-2:2001. These are the probe test, resulting in a probing error value P, and the length test, resulting in a length measuring error E. While this document is technically sound, it leaves some questions unanswered. For example, if a manufacturer is having difficulty meeting the MPE for an instrument, are they permitted to bring very low-uncertainty reference artifacts to the test? This would not improve the CMM performance, but would reduce the test uncertainty, thereby possibly allowing CMM acceptance within the default rule of 14253-1.

RECENT ACTIVITY

Although the initial work described here is best known to the CMM community through working group 10, it is recognized that the general concepts surrounding test uncertainty are not particular to CMMs. To this end, the concepts of test uncertainty have been introduced to working group 4 (uncertainty). It is thought that the main topic of test uncertainty can be described in documents from this working group, and that specific instrument tests and their uncertainty can be developed by the working groups responsible for those instruments.

The uncertainty contributors that are part of the test uncertainty are, as indicated earlier, those which are associated with the testing equipment and its use in the test. The newly introduced Tester's Responsibility Principle, or TRP, is a formalization of this selection process, where only the uncertainty that can be attributed to the person doing the test (the tester) is counted toward that test uncertainty. The repeatability of the CMM is under examination, but is not the responsibility of the tester – it is part of the CMM. For this reason, repeatability of the CMM is not included in the test uncertainty. The greatest concern about the tester's responsibility principle is that the use of the principle leads to discarding uncertainty contributors, which is in violation of the GUM. If we are in violation of the GUM, we can't really call the result an uncertainty. This leaves us with the interesting problem that test uncertainty (as determined using the TRP) might not be a GUM-compliant uncertainty.

The issue of "being a real uncertainty" brings us back to considering the measurand whose uncertainty we are trying to determine. Uncertainty necessarily has a measurand for which the uncertainty is applied. Perhaps – if we are clever – we can determine a measurand for which the uncertainty <u>is</u> the test uncertainty. There have been some false starts in this area, such as stating that the appropriate measurand is the test result (E, for example) at a particular point in time. This seems to be an attractive solution, as the E value represents a real error, and the idea of uncertainty can fit in nicely. The problem is that the true value of the measurand would seem to be the worst error in the CMM volume, which will probably never be measured. This, I believe is an area, where further work has the potential to be very valuable.

NEXT STEPS

There are two additional subject areas open to further work, and we hope to make some progress in these areas, with the help of the experts in the standards community, and experts like those at this conference.

The first project is to attempt to find meaningful language to describe this quantity (referred to here as test uncertainty) and to develop a consistent vocabulary relating to uncertainty in the instrument testing and calibration process. This is not an easy task, because a scan of literature in testing and metrology will reveal that all of the words related to testing, calibration, and uncertainty have been used more than once, and often in conflicting ways. While there are no huge fans (I believe) of the term "test uncertainty" we have yet to find a suitably concise and accurate term to replace it.

The second area in which we would like to extend the current research is in overcoming barriers to the experimental evaluation of test uncertainty. It initially seems that simply running some of the classic CMM acceptance tests (ball bar, step gage, etc.) would reveal different errors when measured at different times, perhaps by different operators. The problem with this method is that the actual CMM performance and repeatability is always folded into the result, which can easily mask the actual effects of test uncertainty. It may be that the best (or only) methods to perform this analysis of test uncertainty is though software simulation, where one contributor at a time can be varied.

ACKNOWLEDGEMENTS

This work draws on the extensive efforts of the members of WG10 who have worked in this area, especially Alessandro Balsamo and Steven Phillips. The authors are pleased to acknowledge the financial support for this work by the National Science Foundation (CMMI-0237501). Any opinions, findings and conclusions or recommendations expressed in this material are those of the authors and do not necessarily reflect the views of the National Science Foundation. In addition, the support of this work and related work by the UNC Charlotte Center for Precision Metrology and its industrial affiliates is gratefully acknowledged.

REFERENCES

[1] ISO 14253-1:1998, Geometrical Product Specifications (GPS) – Inspection by measurement of workpieces and measuring equipment – Part 1: Decision rules for proving conformance or non-conformance with specifications.

[2] ISO 10360-2:2001, Geometrical Product Specifications (GPS) – Acceptance and reverification tests for coordinate measuring machines (CMM) – Part 2: CMMs used for measuring size.

[3] ISO/TS 23165:2006, Geometrical Product Specifications (GPS) – Guidelines for the evaluation of coordinate measuring machine (CMM) test uncertainty.

[4] B89.7.3.1 – 2001: Guidelines for Decision Rules: Considering Measurement Uncertainty in Determining Conformance to Specifications

TEST UNCERTAINTY RATIO (TUR)

Samira Khanam, and Edward Morse
Center for Precision Metrology
University of North Carolina at Charlotte
Charlotte, NC, USA

INTRODUCTION

Manufacturing industries play a significant role in the economy of many countries over the world, including the US. Manufacturing companies' success depends on the production of good quality products. Precise measurement systems are essential to verify the quality of the product. Every measurement process contains variations, just as each manufacturing process does. Manufacturing variations need to be checked by the measurement tools. Measurement tools need to be verified also to insure the best quality of the products. If the variations of the measurement system are high enough, it may affect the whole manufacturing company, as the cost of poor product quality affects the entire manufacturing enterprise. So it is essential for a manufacturing company to have a powerful system to analyze measurement systems. One such measurement analysis tool is the Test Uncertainty Ratio (TUR).

Test Uncertainty Ratio (TUR) is the ratio of the Tolerance to the Uncertainty for a specific measurand. It will provide the information about the accuracy and precision of the system, which include repeatability, reproducibility, etc. One purpose of this paper is to give some industrial guidance on how to use TUR.

$$TUR = \frac{Tol.}{U}, \text{ where}$$

Tol.= Tolerance of the product which is in manufacture's specification, and
U= Uncertainty for the specific task.

One method of evaluating the expanded measurement uncertainty for a task is to combine the short-term variability of the system with a bias of the system, as shown below.

$$U = |bias| + 2\sigma_{meas}$$

It is common to require that the TUR value be 4:1 or higher, where a larger value of the TUR corresponds to a better performing measurement system.

DEFINITIONS

To understand TUR, it is necessary to know the definition of some terms in detail. This paper will discuss these first: accuracy, bias, precision, uncertainty, and task-specific uncertainty.

Accuracy *(from VIM)*
Accuracy is the closeness of agreement between a measured quantity value and a true quantity value of a measurand.
The measurand is a quantity intended to be measured. The concept 'measurement accuracy' is not quantitative and is not given a numerical quantity value. A measurement is said to be more accurate when it offers a smaller measurement error.

Bias (*from Industry*)
The bias, or offset, is how we quantify accuracy. Bias is the difference between the average value of all the measurements (μ) and the true value (μ_0). Bias is a measure of the amount by which a tool is consistently off target from the true value. Bias can be positive or negative.

$$Bias = \mu - \mu_0$$

Because the exact true value is not possible to know, the 'best' estimate of the parameter being measured may be provided by the National Institute of Standards and Technology (NIST) or another national metrology institute (NMI). It can be used as a reference value, with a suitably low uncertainty.

Precision (*from VIM*)
Precision is the closeness of agreement between indications or measured quantity values obtained by replicate measurements on the same or similar objects under specified conditions.
Measurement precision is usually expressed numerically by measures of imprecision, such as standard deviation, variance, or coefficient of variation under the specified conditions of measurement. The 'specified conditions' can

be, for example, repeatability conditions of measurement.

Measurement Uncertainty (from *VIM*):
parameter, associated with the result of a measurement, that characterizes the dispersion of the values that could reasonably be attributed to the measurand.

Measurement Uncertainty (from *industry*):
Measurement uncertainty is a parameter which describes the measured values of a quantity which is close to the true value of that quantity.

Task Specific Uncertainty [1]:
Task specific uncertainty is a parameter which is associated with the measured value of a specific task for specific measurement procedure.

TUR CONTRIBUTORS

After knowing the basic definitions of terms, it is important to know the contributors that affect the TUR, which will help to calculate TUR. Figure 1 shows the contributors to the task specific uncertainty, which is necessary to find the TUR.

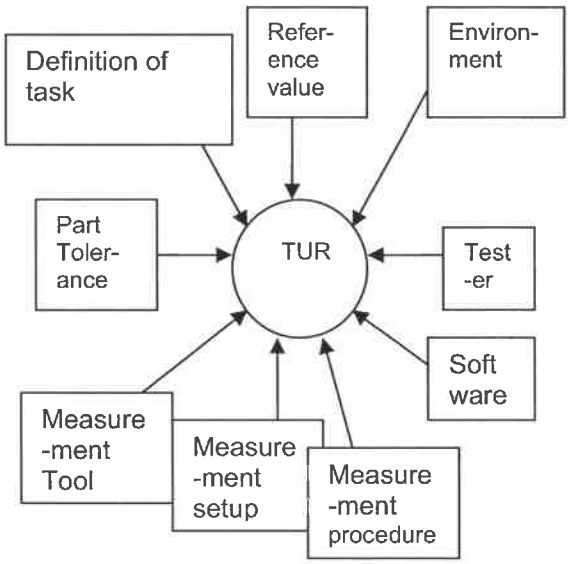

Figure 1: Contributors to TUR

Definition of task: The task needs to be determined first. It may be size, true position or any other characteristic of interest. For every task one need to calculate TUR individually and tolerance need to be determined separately. For example if one need to calculate TUR for both size and true position, then the tolerance values for each should be known separately and used in the appropriate TUR calculation.

Part Tolerance: The tolerance for every task needs to known to calculate TUR. In the case where one is trying to determine the limiting tolerance value that can be inspected, this can be obtained by using the lowest acceptable value of TUR and the task-specific uncertainty for that measurand.

Reference value: The reference value may be needed to calculate the bias for a particular measurement. The uncertainty of this value will be lowest if it is obtained from an NMI, but a reference value with a suitably low uncertainty from another reliable source is acceptable.

Environment: Temperature, vibration, dust, etc may influence the value of Uncertainty. So these factors need to be taken into consideration when measuring the part.

Measurement Tool: The ability of the measurement tool to measure the part accurately has the greatest influence on the value of TUR. However, it is a mistake to think that this is the only source of uncertainty.

Measurement set up: If the set up of both the part and the tool is not perfect, the measurement result can be vary.

Measurement procedure: One need to use the measurement procedure as defined for each measurement tool.

Software: The measurement results depend on the software, analysis tool of the measurement tool.

Tester: Test results depend on how expert the tester is.

The contributors described above have influence on the results of a measurement system. So the *Task Specific Uncertainty* result will be influence by this. As a result TUR value will change.

OTHER METRICS

The P/T ratio is another metric used in the industries (such as Intel) to find the measurement capability of the metrology tool. Below P/T is described and compared with TUR also to find the reliability of TUR.

The P/T Ratio (*Industry*)
The capability of the measurement system is quantified by computing the P/T (Precision-to-Tolerance) Ratio.

For two-sided specifications (those which have both USL and LSL):

$$P/T = \frac{6s_{ms}}{USL - LSL} x100\%,$$

where ms=measurement system

For one-sided specs (those which have either USL or LSL, or if no spec limits exist):

$$P/T = \frac{3s_{ms}}{TOL} x100\%,$$

where TOL = (Process Mean or Target – LSL) for LSL only, or (USL – Process Mean or Target) for USL only.

For this measure:
- Small values of P/T are desirable.
- P/T ≤ 30%: Measurement system capable.
- P/T > 30%: Measurement system not capable (not precise enough)

EXAMPLE
We now give an example comparing the measurement capability of metrology tools.

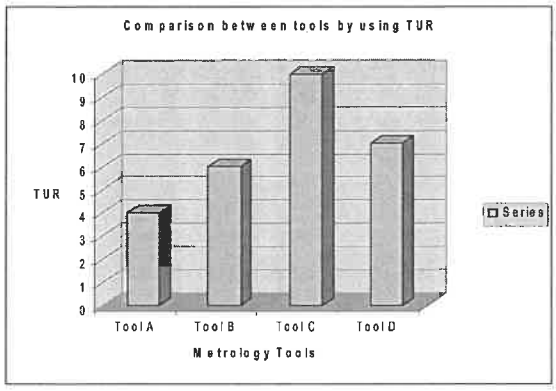

Figure 2. Measurement capability comparison

Figure 2 shows a graph where we can compare the measurement capability of four metrology tools. Tool C has the highest TUR value of 10. It means the measurement capability of this tool is better than the others. The measurement capabilities of other tools are ordered as follows Tool D, Tool B, and tool A. Comparing the P/T values for these tools reveals that Tool C will give smallest value, and then consequently Tool D, Tool B and tool A.

EXPERIMENTAL COMPARISON
Experiments have been done to compare the TUR and P/T ratio for different measurement tasks. Two blocks, one made of steel and the other of aluminum, were used for these calculations. Different numbers of points were taken on a circular feature (6, 16 and 30 points), and different numbers of points were taken on the datum features. In each case, 4 points were taken on Datum A (the top); and the either 2 or 4 points were taken on Datums B and C (the sides). One example of this is shown in Figure 3 below.

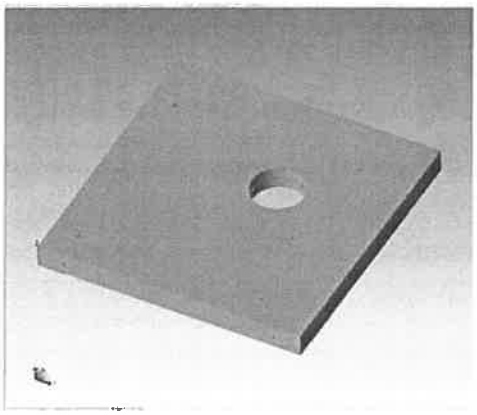

Figure 3 Datum A - 4 points, Datum B - 2points, Datum C - 2 points

In addition to evaluating the position of the circular feature, we also measured the overall width of the block, using 4, 12, or 30 points on each side. The measurement setup for these parts is shown in Figures 4 and 5.

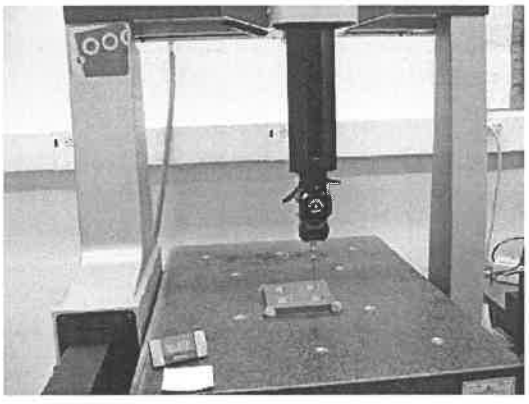

Figure 4: Steel block on CMM

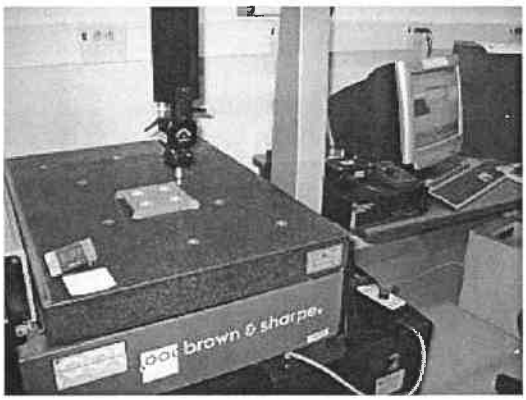

Figure 5: Aluminum block on CMM

Results: Position Tolerance

The experimental results for the position tolerance are shown below. The results for the steel and aluminum parts were nearly identical, so the aluminum part results are omitted here. The value for the position callout was a 25μm diameter tolerance zone for the axis of the feature.

Tables 1 and 2. Steel Block position values

Uncertainty and TUR with datum points 4,2,2 for steel plate by using CMM			
#of points on Circle	**2σ (μm)**	**U (μm)**	**TUR**
6	2.17	26.61	1:1
16	2.45	26.10	1:1
30	1.56	27.77	1:1

Uncertainty and TUR with datum points 4,4,4 for steel plate by using CMM			
#of points on Circle	**2σ (μm)**	**U (μm)**	**TUR**
6	1.49	26.63	1:1
16	1.64	27.13	1:1
30	1.89	27.29	1:1

We can see in the tables above that the 2σ spread of data from multiple measurements is improved by taking more points on the datum features, but because the bias in the results is so large, by comparison, this improvement is not reflected in the TUR values.

The next table shows the P/T ratio for these measurements, along with the bias in both X and Y that results in the unacceptable values for TUR. Note that the P/T alone gives values that appear reasonable.

TABLE 1. P/T and Bias for position data

P/T and bias with datum points 4,4,4 for steel plate by using CMM			
#of points on Circle	**P/T**	**Bias (in X and Y) (μm)**	
6	17.88%	21.6	9.6
16	19.68%	22.2	8.7
30	22.68	22.1	8.0

Results: Size Tolerance

For this experiment different number of points were taken from left to right to find the distance between these 2 sides. The number of points was 4, 12 and 30 points. Figure 6 below shows the measurement points for the 12 point case.

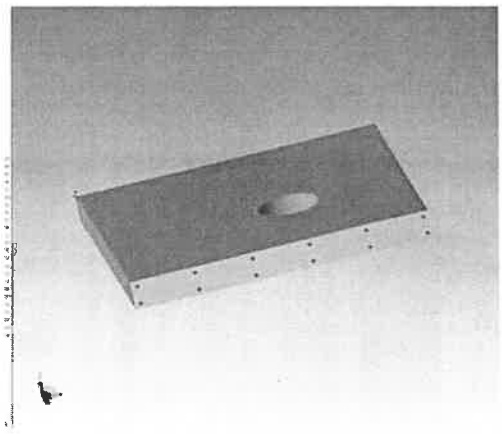

Figure 6. Test part with measurement points

The tables below show both capability measures for the steel plate and the aluminum plate. In each case we can see that the bias introduced by uncorrected thermal changes, and the errors introduced by the point placement in the 4 point case result in a bias that dominates the short term variability of the measurements.

Of course, an uncorrected bias is not something that we would expect to happen in ordinary measurements. However, if we do not know the extent to which certain errors occur (thermal

drift, loose fixturing, etc.), this uncorrected bias may be introduced. The message that is hidden in these data is that a procedure that does not capture the bias, but only quantifies the repeatability, is at risk of over-estimating the capability of the measurement system. One such method that does not capture bias in repeated measurements is a GR&R study.

Table 4: Size Tolerance of Steel Plate

U, TUR, P/T, Bias for Steel plate using CMM					
#of points	**2σ (µm)**	**U (µm)**	**TUR**	**P/T**	**Bias**
4	.843	25.44	2:1	5.05%	24.605
12	1.13	3.71	13:1	6.78%	2.58
30	1.05	7.13	7:1	6.3%	6.08

Table 5: Size Tolerance of Aluminum Plate

U, TUR, P/T, Bias for Aluminum plate using CMM					
#of points	**2σ (µm)**	**U (µm)**	**TUR**	**P/T**	**Bias**
4	.632	41.28	1:1	3.79%	41.1
12	.906	9.69	5:1	5.4%	9.06
30	1.93	10.87	5:1	11.58%	8.94

CONCLUSIONS

The steel and aluminum plates were used to calculate TUR and P/T to show how different factors – such as part material – can influence the results. After analyzing the data it was found that the TUR for position tolerance of a circular feature is the same in both materials. We also show that the TUR utilizes both the bias and precision, while the P/T is only using precision. For this reason, we need to separately check the accuracy (bias) using a reference value. For different numbers of points, the TUR of position tolerance does not change because this measurement is dominated by the bias. But, for the size tolerance with increasing number of points, the measurement gives a higher TUR. The steel plate has a higher TUR than the aluminum part. These two results are sensible, as the steel responds more slowly and to a lesser extent to temperature changes. Because this experiment was done with only one metrology tool, we are comparing the capability of measuring different part materials for different measurands. The same type of measurement capability study could be used for the same part on different measurement tools.

REFERENCES

[1] R. Wilhelm, R. Hocken and H. Schwenke, Task specific uncertainty in coordinate metrology, Keynote paper, Annals of CIRP, Vol. 50/ 2 (2001), pp. 553–563

[2] International Vocabulary of Basic and General Terms in Metrology, 2nd ed., (1993).

NEW CONCEPTS IN UNCERTAINTY WHEN CALIBRATING MEASURING EQUIPMENT

James G. Salsbury
Mitutoyo America Corporation
Aurora, Illinois, USA

INTRODUCTION

The goal of this paper is to introduce new concepts in measurement uncertainty [1] when calibrating, testing, or verifying indicating measuring instruments. The examples are taken from the field of dimensional metrology, such as micrometers and coordinate measuring machines (CMM), but the concepts most likely have application in other fields of metrology. In order to introduce these new measurement uncertainty ideas, a new structure is introduced that clarifies the difference between verification and calibration of indicating measuring instruments. In addition, the difference between sampling measuring errors and assigning measuring errors will be discussed. Numerical examples are included along with some practical recommendations for industry.

INDICATING MEASURING INSTRUMENTS

The VIM [2] defines a *measuring instrument* as either being an *indicating measuring instrument* or a *material measure*. These VIM terms and definitions are used in this paper as they provide a useful distinction between these types of measuring instruments. This paper is concerned with the calibration of indicating measuring instruments in the dimensional metrology field including, for example, coordinate measuring machines (CMM) and micrometers. Examples of material measures in the dimensional metrology field include gage blocks, line scales, and ring gages. When properly calibrated, both material measures and measuring instruments can be used as *measurement standards*. In this paper, the term *material standard* [3] will be used for material measures that are used as measurement standards.

The calibration and associated measurement uncertainty of material standards are of particular importance for purposes of metrological traceability. The research literature is rich with measurement uncertainty examples for the calibration of material standards (for example, see [4-5]). The National Metrology Institutes (NMI), which often provide the highest level of calibrations and uncertainty of material standards, have contributed much of this uncertainty work. In contrast, measurement uncertainty examples for the calibration of indicating measuring instruments are usually only found as informative examples in general uncertainty literature or metrology standards (for example, see [6-8]).

The first document to give detailed treatment to the measurement uncertainty when calibrating or testing indicating measuring instruments is ISO/TS 23165:2006 [9]. This document, written only for CMM use, introduces the concept of *test uncertainty*, which is defined as the uncertainty associated solely with the test equipment and its use in the test. As will be discussed later, this definition varies from prior published uncertainty examples and differs not only in the treatment of uncertainty but also in the concept of what it means to calibrate or test indicating measuring instruments. In this paper, the basic concept of test uncertainty is refined and expanded to indicating measuring instruments in general.

CALIBRATION VERSUS VERIFICATION

The VIM states "verification should not be confused with calibration" and that calibration should not be confused with "verification of calibration". Calibration is defined in the VIM as:

> *operation that, under specified conditions, in a first step, establishes a relation between the quantity values with measurement uncertainties provided by measurement standards and corresponding indications with associated measurement uncertainties and, in a second step, uses this information to establish a relation for obtaining a measurement result from an indication*

The second step in this definition presupposes the use of measurement results. If the "information" satisfies the first step, which essentially requires measurement results with associated uncertainties, and that information is

subsequently used as the calibration, then it is the calibration.

The VIM definition of calibration, though a bit complicated, is very useful. There are situations where only the first step in this definition is met, and in these cases, the measurement results are not a calibration. An example of this type of measurement may occur when using a check standard or other type of quality check. Check standards are often used as a type of verification of calibration, but not as the calibration.

Verification is defined in the VIM as, "provision of objective evidence that a given item fulfils specified requirements". The "item" and the "specified requirements" in this definition could be almost anything, and thus the concept and application of verification is quite broad. One application is the verification of calibration as just discussed. Another application in the metrology field is the verification of an indicating measuring instrument (or one or more of its specific metrological characteristics) to the corresponding maximum permissible measurement error, or MPE. This type of verification is widely used in national and international metrology standards under various names, such as acceptance tests [10], reverification tests [11], conformance tests [12], and performance evaluation tests [13]. All of these "tests" are types of verifications.

The results of a verification test of an indicating measuring instrument to its MPE(s) is usually the "information" that is used to satisfy the second step clause of the definition of calibration. This type of verification is therefore not a verification of calibration but is indeed the calibration. The measurement results of the verification test are initially only the verification of the MPE, but if the results are used as the calibration, then the verification becomes the calibration as well.

For example, consider an outside micrometer that has been verified to conform to its error of indication MPE. There may exist a set or table of measured indications from the verification process, but the user of the micrometer is only concerned that the micrometer conforms to the MPE. The only *measured quantity value* [2] that results from the indications is the conformance to the MPE. This measured quantity value, along with its associated uncertainty, is the only result of the measurement. This measurement result satisfies the first step in the VIM definition of calibration and is subsequently the information that is used to satisfy the second step. The verification of the micrometer becomes the calibration of the micrometer.

SAMPLING VERSUS ASSIGNING

The VIM states "the indication of a material measure is its assigned quantity value". When a material measure is calibrated, the objective of the measurement is the assignment of a value. The VIM also states that the quantity being supplied or reproduced by the material measure is permanent during its use. While the term permanent may be a bit vague, there is an underlying assumption that material measures, and material standards, are stable during their use. This stability assumption becomes part of the definition of the measurand when calibrating material standards. The measurand is defined at specific conditions, for example at a temperature of exactly 20°C, such that it is unique and reproducible, and therefore variation observed in indications when calibrating the material standard is attributed to the measurement uncertainty.

When calibrating an indicating measuring instrument through the use of verification testing, for example to a specific MPE, the nature of the measurand, and its impact on the measurement uncertainty, must be carefully considered. In these cases, the goal of the calibration is not the assignment of values as when calibrating material standards; instead, the measured indications during a verification test are samples of the measurement errors of the indicating measuring instrument under specific conditions. In these cases, the sample measured errors are used only to determine conformance to the MPE.

For indicating measuring instruments, there are two possible objectives of a calibration. In one case, the measurand is the assigned value of the measuring error, and in the second case the measurand is a sample measured error. This concept is captured, using slightly different terminology, by the idea of test uncertainty introduced in ISO/TS 23165 for CMM testing. When a verification test is done on a CMM following ISO 10360-2, the measured indications (or errors) of the CMM are sampled under various conditions. These indications are only intended for use in determining conformance and are not intended to be the assigned values

of the CMM. Much of the variation in the indications is due to errors in the CMM itself. According to ISO/TS 23165, "only those uncertainty components that pertain to the test itself are included in the test uncertainty". In particular, errors introduced by the CMM are not included in the test uncertainty as they are part of the measurand.

Instead of using the test uncertainty terminology, in this paper the distinction is based on whether the measurand is the assigned value of the measuring error or the sampled measured error. The assigned measuring error, for an indicating measuring instrument or one of its metrological characteristics, is the assigned measurement error at some specific position within the measuring range of the instrument and under specific operating conditions. The assigned measuring error could be used for correcting estimated systematic effects in the indicated measuring instrument or for verification purposes. In contrast, the sample measured error is a measured error that is sampled near some nominal position within the measuring range of the instrument and in a sample of the allowable operating conditions of the instrument. The sample measured error is only used for verification purposes and should not be considered as the assigned value. Once a conformance decision has been made, there is no other use for the measurement results, and they are only kept or reported for purposes of historical records.

To highlight the distinction between the assigned value of the measurement error and a sample measured error, consider a CMM that is tested according to ISO 10360-2. Figure 1 shows example measured indications from a portion of the results from the CMM testing. The purpose of this verification test is to determine conformance to the CMM specification for length measurements, MPE_E. The measuring errors of the CMM are sampled by taking indications on various length material standards, for example gage blocks, under any of the allowable operating conditions defined by the CMM manufacturer for this particular test.

The indications shown in Figure 1 are sample measured errors. As such, there is no attempt to assign these results to the CMM or to claim these indications are indeed the true errors of the CMM. There is also no expectation of permanency to the results. The lack of permanency, or repeatability, of the test results is actually part of the purpose behind the standardized testing procedure – namely the three repeat measurements taken at each length (as required by ISO 10360-2). The measurand is the sampled measured error, and the true value of the measurand depends on the specific conditions of the CMM at that moment in time. As the errors introduced by the CMM change, due to many factors including inherent mechanical stability or the influence of ambient temperature, the true value of the measurand is therefore also changing.

If the purpose of CMM testing were to assign measuring errors, then a very different procedure would most likely be used. For example, the specific location of the material standard used for the measurements would be more carefully established. In addition, an average of multiple indicated readings would likely be used to better determine the measurement error at a single position. The probing system and thermal conditions would

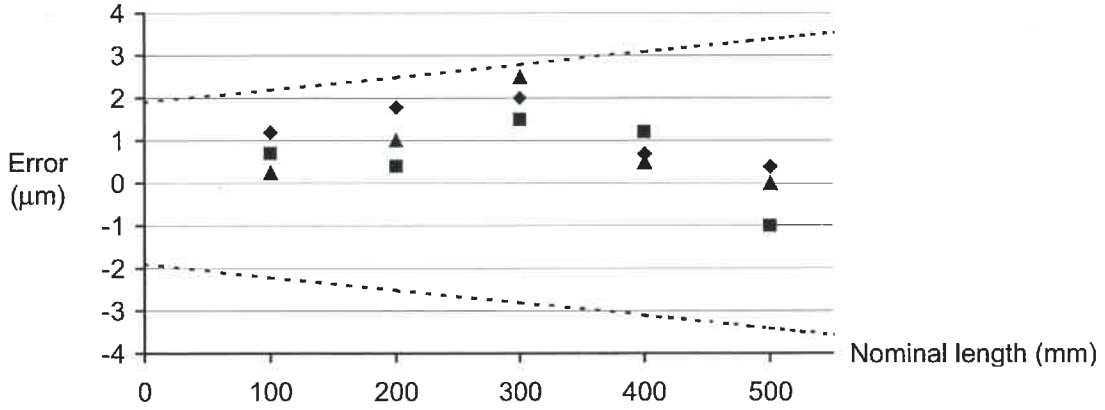

FIGURE 1. Sample measured errors for CMM verification to ISO 10360-2. The dotted lines represent the MPE_E =1.9+3L/1000 mm. The results are used to determine conformance but are not assigned to the CMM.

probably also be selected with greater care. Any of the allowable operating conditions that could possibly influence the measured errors would have to be considered, including the long-term stability of the CMM itself. When the measurand is the assigned value of the measuring error, any influence on the variation of the indications has to be considered in reporting the measurement results. Similarly, there is a longer list of influence quantities to the measurement uncertainty that must be considered when the measurand is the assigned value of the measuring error then when the measurand is the sample measured error. While the measurement procedure used to sample a measurement error may or may not be different than that used to assign the measurement error, in either case, the measurement uncertainty can be very different.

CMM TEST UNCERTAINTY

The term "test" is used in ISO/TS 23165 in the sense where the test is a verification of a specific MPE of the CMM. This test uncertainty is a specific example of the measurement uncertainty when the measurand is a sample measured error, or for short, the *sample uncertainty*, U_S. Prior to the publication of ISO/TS 23165, it was not uncommon for the measurement uncertainty of CMM verification to be based on the measurand being the assigned value of the measuring error, or for short, the *assignment uncertainty*, U_A (e.g., see [14]).

ISO/TS 23165 is specific on what influence factors are to be considered in the test uncertainty (or sample uncertainty). Assuming issues such as fixturing and alignment are properly managed, the only significant sources of uncertainty to consider for the length accuracy test, limited by MPE_E, are shown in Table 1. In contrast, Table 1 also shows example values when the assignment uncertainty is considered.

As can be seen in Table 1, only the sources of uncertainty directly under the control of the party who performs the test, the so-called *tester* in ISO/TS 23165, are included in the uncertainty analysis. Any other observed variation in the measured indications of the verification test is attributed to the CMM and is therefore included in the measurand and not in the uncertainty. Most environmental issues are also not included in the test uncertainty as a CMM is verified on-site, as the tester has no control over the environment. More importantly, however, is that CMM accuracy specifications, including the MPE_E, are defined over an allowable range of operating conditions, including temperature. When the measurand is a sample measured error, the sample is allowed to be taken under any allowable operating conditions for which an MPE applies. The value of a sample measured error may change when the operating conditions change, but this variation is limited by the MPE, and is not part of the measurement uncertainty.

TABLE 1. Uncertainty when calibrating a CMM with a built-in temperature compensation system at a length of 200 mm (also see [14]).

Uncertainty Source	Standard Uncertainty (μm)	
	Assignment (U_A)	Sample (U_S)
Step gage calibration	0.09	0.09
Repeatability	0.30	---
Measurement of CMM scale temperature	0.28	---
Measurement of step gage temperature	0.25	---
Thermal expansion coefficient of CMM scales	0.08	---
Thermal expansion coefficient of step gage	0.06	0.06
Combined and expanded uncertainty using k=2	1.0	0.2

In Figure 2(a), the three repeat indications from the 200 mm length in Figure 1 are shown, along with bars representing the sample uncertainty. The values in this example were specifically chosen to highlight that the variation between the three indications could be larger than the sample uncertainty. As discussed earlier, there is no expectation of permanency to the results. Figure 2(b) shows an example when the same measured errors from Figure 2(a) are used to determine the assigned value of the CMM. In this case, the indications are averaged together, as an example, to determine the assigned value of the measuring error, and the measurement uncertainty is larger to include additional

sources of variation. The numerical values of both uncertainties are taken from Table 1.

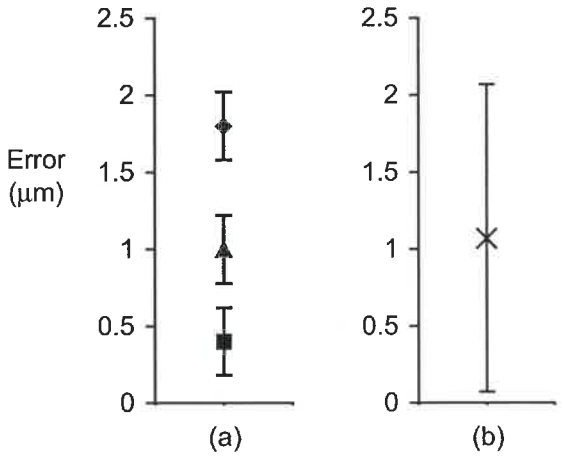

FIGURE 2. The sample measured errors from the 200 mm length of the CMM verification in Figure 1 are shown in (a) with the associated sample uncertainty U_S. If the goal is assignment of the values, then one approach is shown in (b) with the associated assignment uncertainty U_A.

MICROMETER CALIBRATION

Like the CMM, another common calibration in dimensional metrology is that of an outside micrometer. Complete measurement uncertainty analyses for the calibration of these indicating measuring instruments can be found as examples in various authoritative documents (for example [6-8]). Though it is not stated as such, the uncertainty examples found in these various documents are the assignment uncertainty and not the sample uncertainty.

Table 2 shows an example uncertainty analysis for the calibration of the error of indication of a vernier micrometer following ASME B89.1.13 [7]. The numerical values shown in Table 2 are taken from this American standard. To estimate U_A any sources of variation in the assigned error must be considered. The assigned errors of the micrometer, like that of the gage block, are considered permanent during use. As shown in Table 2, when estimating U_A, sources of uncertainty such as the micrometer resolution and the observed repeatability of the measurement results are usually included.

Table 2 also shows an estimate of U_S for this same micrometer calibration. As the resolution of the micrometer is an inherent part of the micrometer it is not part of the sample uncertainty. The contribution of the so-called repeatability is more difficult to estimate. Repeatability, as used in this example from ASME B89.1.13, is a Type A evaluation [1] of uncertainty that is determined by performing repeated indications and calculating the standard deviation. Repeatability is not really an influence quantity; it is the result of an experimental study. The purpose of the study is to capture the impact of all the "other" influence quantities that are not already included in the uncertainty analysis. For the sample uncertainty, the typical repeatability study needs to be reconsidered. If the observed non-repeatability is due to the measuring errors of the micrometer, then that variation is not part of U_S. If the observed non-repeatability is due to the testing procedure, for example incorrect use of the force controlling ratchet on the micrometer, then that variation is part of the U_S. For example purposes here, the repeatability is assumed to be negligible for U_S, though that may not necessarily always be the case.

TABLE 2. Uncertainty when calibrating a 0-25 mm vernier micrometer (based on [7]).

Uncertainty Source	Standard Uncertainty (μm)	
	Assignment (U_A)	Sample (U_S)
Gage Blocks	0.08	0.08
Repeatability or Resolution	0.45	---
Difference in coefficients of thermal expansion	0.05	0.05
Difference in temperature	0.17	0.17
Combined and expanded uncertainty using k=2	1.0	0.4

Unlike the CMM example, there are additional temperature related sources of uncertainty for the micrometer calibration that are included in both U_S and U_A. The MPE for the error of indication of the micrometer is defined only at exactly 20°C, and since the tester can control the testing environment (for example, by bringing the micrometer into a temperature controlled laboratory), then these additional sources of uncertainty are included in U_S.

REPORTING RESULTS

A micrometer is usually verified to some MPE, and like a CMM, this verification is the calibration. There is generally no need to assign values to the measuring errors when calibrating micrometers, as those assigned values would not be used. When measuring with a micrometer it is generally not the intention of the calibration certificate to be used as a table of correction values (if such results are even reported). Micrometers, and practically all indicating measuring instruments in the dimensional metrology field, are calibrated by verification to specific MPE values. In these cases, the measurand is a sample measured error, not the assigned value of the measuring error, and therefore the sample uncertainty should be used in the verification/calibration process.

Following the VIM, a measurement result includes both a measured quantity value and the associated measurement uncertainty. When the measurand is the assigned value of the measuring error, the measurement result consists of an assigned value and U_A. When the measurand is a sample measured error, and verification of an MPE has been determined, then the measurement result is the MPE and U_S.

To avoid confusion in practice, it is recommended that some type of note be added to calibration certificates when the reported measured indications are sample errors and not assigned values. For example:

> *These indications are a sample of the measuring errors of this indicating measuring instrument and are not being assigned to this instrument. Sampled measuring errors may be different under different allowable operating conditions.*

FUTURE WORK

The publication of the GUM in 1995 triggered the start of formal estimation of measurement uncertainty across the entire metrology field. While much has been published in this area, there is still very little that specifically treats the calibration of indicating measuring instruments. It is hoped that this paper, and documents like ISO/TS 23165, will prompt others to reconsider the complexity of this situation and begin new research and standards in this area.

REFERENCES

[1] ISO/IEC Guide 98-3:2008, Uncertainty of measurement – Part 3: Guide to the expression of uncertainty in measurement (GUM:1995).

[2] ISO/IEC Guide 99:2007, International vocabulary of metrology – Basic and general concepts and associated terms (VIM).

[3] ISO 10360-1:2000, Geometrical Product Specifications (GPS) – Acceptance and reverification tests for coordinate measuring machines (CMM) – Part 1: Vocabulary.

[4] Doiron T, Stoup J. Uncertainty and dimensional calibrations. Journal of Research of NIST. 1997;102(6):647-676.

[5] Decker J E, Ulrich A, Pekelsky J R. Uncertainty of Gauge Block Calibration by Mechanical Comparison. Measure, Journal of Measurement Science. 2008; 3(4):30-42.

[6] ISO/TS 14253-2:1999, Geometrical Product Specifications (GPS) – Inspection by measurement of workpieces and measuring equipment – Part 2: Guide to the estimation of uncertainty in GPS measurement, calibration of measuring equipment and product verification.

[7] ASME B89.1.13-2001, Micrometers.

[8] EA-4/02, Expression of the Uncertainty of Measurement in Calibration. European co-operation for Accreditation. 1999.

[9] ISO/TS 23165:2006, Geometrical Product Specifications (GPS) – Guidelines for the evaluation of coordinate measuring machine (CMM) test uncertainty.

[10] ASME B89.7.3.1-2001, Guidelines for Decision Rules: Considering Measurement Uncertainty in Determining Conformance to Specifications.

[11] ISO 10360-2:2001, Geometrical Product Specifications (GPS) – Acceptance and reverification tests for coordinate measuring machines (CMM) – Part 2: CMMs used for measuring size.

[12] ISO 14253-1:1998, Geometrical Product Specifications (GPS) – Inspection by measurement of workpieces and measuring equipment – Part 1: Decision rules for proving conformance or non-conformance with specifications

[13] ASME B89.4.1-1997, Methods for Performance Evaluation of Coordinate Measuring Machines.

[14] Salsbury J. Uncertainty and decision rules in CMM calibration. 2006 NCSL International Workshop and Symposium.

Author Index

Bastam, Dirk 11
Bryce, E. A. Tony 36
Burge, James H. 20
*Burton, Roger N.** 41
*Doiron, Theodore D.** 40
Donker, Rilpho L. 15
Evans, Christopher J. 7
Howard, Lowel P. 3
Jusko, Otto E. 11
Khanam, Samira A. 42, 45
Morse, Edward P. 42, 45
Oh, Chang Jin 20
Parks, Robert E. 20
Pratt, Jon R. 3
Reimann, Helge 11
Salsbury, James G. 50
Smith, Craig 7
Smith, Douglas T. 3
Soobitsky, James A. 7
Spaan, Henny A. M. 15
Stoup, John R. 26
Su, Peng 20
Widdershoven, Ivo 15
Woynar, Michael 7

** Extended abstract unavailable at press time*

ASPE 2009 Sustaining Corporate Sponsors

3M Company
St. Paul, MN 55144
Phone: (651) 737-3790
www.mmm.com

ADCOLE Corporation
669 Forest Street
Marlborough, MA 01752
Phone: (508) 485-9100
Fax: (508) 481-6142
www.adcole.com

Aerotech, Inc.
101 Zeta Drive
Pittsburgh, PA 15238-2897
Phone: (412) 963-7470
Fax: (412) 963-7459
www.aerotech.com

Ametek Precitech, Inc.
44 Blackbrook Road
Keene, NH 03431
Tel: (603) 357-2511
Fax: (603) 358-6174
www.precitech.com

Chardon Tool
115 Parker Court
Chardon, OH 44024
Phone: (440) 286-6440
Fax: (440) 286-7165
www.ChardonTool.com

Corning Tropel Corporation
60 O'Connor Road
Fairport, NY 14450
Phone: (585) 388-3500
Toll-free: (888) 4-TROPEL
www.tropel.com

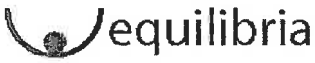

Equilibria
472 Amherst Street
Unit 25
Nashua, NH 03063
Phone: (603) 880-7722
www.eqlib.com

K & Y Diamond
2645 Diab St. Laurent
Quebec H4S 1E7
CANADA
Phone: (514) 333-5606
Fax: (514) 339-5493
www.kydiamond.ca

Fabreeka International, Inc.
P.O. Box 210
1023 Turnpike Street
Stoughton, MA 02072
Phone: (781) 341-3655
Toll-free: (800)-322-7352
www.fabreeka.com

Lion Precision
563 Shoreview Park Road
St. Paul, MN 55126-7014
(651) 484-6544
(651) 484-6824
www.lionprecision.com

ASPE 2009 Sustaining Corporate Sponsors

Makino
7680 Innovation Way
Mason, OH 45040
Phone: (513) 573-7200
Fax: (513) 573-7360
www.makino.com

Mitutoyo America Corporation*
945 Corporate Boulevard
Aurora, IL 60504-9102
Phone: (630) 723-3619
Fax: (630) 978-6471
www.mitutoyo.com

Moore Tool Company, Inc.
800 Union Avenue
Bridgeport, CT 06607-0088
Phone: (203) 366-3224
Fax: (203) 366-5694
www.mooretool.com

New Way Precision, Inc.
4009-I Market Street
Aston, PA 19014
Phone: (610) 494-6700
Fax: (610) 494-0911
Toll-Free: (800) 394-1046
www.newwaybearings.com

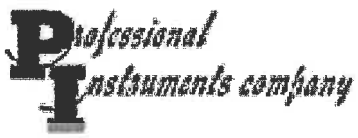

Professional Instruments Company
7800 Powell Road
Hopkins, MN 55343
Phone: (952) 933-1222
Fax: (952) 933-3315
www.airbearings.com

Trust Automation, Inc.
143 Suburban Road
San Luis Obispo, CA 93401
Phone: (805) 544-0761
Fax: (805) 544-4621
www.trustautomation.com

Zygo Corporation
Laurel Brook Road
Middlefield, CT 06455-0448
Phone: (860) 347-8506
Fax: (860) 347-8372
Toll-free: (800) ZYGO-NOW
www.zygo.com

ASPE 2009 Corporate Sponsors

Center for Precision Metrology
University of North Carolina at Charlotte
Charlotte, NC 28223
(704)-687-8499

Contour Fine Tooling, Inc.
Marlborough, NH 03455
(603) 876-4908

Corning Inc.
Corning, NY 14831
(607) 974-3842

Cranfield Precision
Division of Cinetic Landis Lund, Ltd.
Cranfield, Bedford MK43 OJR, England
+44-1234-754222

euspen
Cranfield University
Bedford, MK43 OAL, United Kingdom
+44-1234-754024

Nano Corporation
Tokyo 144-0042, Japan
+81-3-5735-6631

Philips Applied Technologies
San Jose, CA 95131-1706
(408) 991-2261

Reflexite Precision Technology Ctr.
West Henrietta, NY 14586
(585) 272-0290

Seagate Technology
Scotts Valley, CA 95066
(831) 439-3697

Singulus Mastering, B. V.
Eindhoven, The Netherlands
+31-40-7501-400

StarragHeckert, Incorporated
Hebron, KY 41048
(859) 534-5201

Veeco
Tucson, AZ 85706-7123
(520) 741-1044